DOI: 10.1070/RCR4798

Nanocomposites based on tubular and onion nanostructures of molybdenum and tungsten disulfides: inorganic design, functional properties and applications

Alexander Yu Polyakov,[a] Alla Zak,[b] Reshef Tenne,[c] Eugene A Goodilin,[a, d] Konstantin A Solntsev [a, e]

[a] *Faculty of Materials Science, Lomonosov Moscow State University*
Leninskie Gory 1, stroenie 73, 119991 Moscow, Russian Federation
[b] *Faculty of Sciences, Holon Institute of Technology*
Golomb St. 52, Holon 5810201, Israel
[c] *Department of Materials and Interfaces, Weizmann Institute of Science*
Herzl St. 234, Rehovot 76100, Israel
[d] *Department of Chemistry, Lomonosov Moscow State University*
Leninskie Gory 1, stroenie 3, 119991 Moscow, Russian Federation
[e] *Baikov Institute of Metallurgy and Materials Science*
Leninskiy prosp. 49, 119334 Moscow, Russian Federation

The review concerns the development and the state-of-the-art in studies on the surface modification methods aimed at fabricating promising nanocomposites based on multilayer inorganic tubular and onion (fullerene-like) MoS_2 and WS_2 nanostructures. The synthetic details and structural features of these materials are considered. Considerable attention is paid to targeted functionalization of molybdenum and tungsten disulfide nanostructures and to fundamental principles that underlie their ability to chemical interactions. The functional properties and applications of the obtained materials are described.
The bibliography includes 183 references.

Contents

1. Introduction 252
2. Structural features of MoS_2 and WS_2 nanotubes and onion nanostructures 252
3. Synthesis of MoS_2 and WS_2 nanotubes and onion nanostructures 255
4. Principles and methods for modification of tubular and onion nanostructures of molybdenum and tungsten disulfides 259
5. Applications of nanocomposites based on tubular and onion nanostructures of molybdenum and tungsten disulfides 265
6. Conclusion 267

A.Yu.Polyakov. Engineer, PhD student, Faculty of Materials Science, MSU.
Telephone: +7 (495) 939 – 4609, e-mail: a.yu.polyakov@gmail.com
Current research interests: metal and metal oxide nanoparticles; metal – semiconductor structures including nanotubular composites; layered 2D materials; optical and chemical sensors.
A.Zak. Professor, Head of the Laboratory for Synthesis and Investigations of Nanomaterials, Faculty of Sciences, Holon Institute of Technology, Israel. Telephone: + (972) 3502 – 6802, e-mail: alzak@hit.ac.il
Current research interests: laboratory-scale and industrial synthesis of WS_2 and MoS_2 nanotubes and fullerene-like structures; studies on physicochemical properties of these materials; design of reinforced polymeric nanocomposites based on disulfide materials.
R.Tenne. Member of the Israel Academy of Sciences and Academia Europaea, Research Professor, Department of Materials and Interfaces, Weizmann Institute of Science, Israel.
Telephone: +(972) 8934 – 2394, e-mail: reshef.tenne@weizmann.ac.il
Current research interests: synthesis of inorganic nanotubes, investigations of physical phenomena in and applications of inorganic nanotubes and fullerene-like nanostructures; chemistry of disulfide materials, design of novel materials and composites, catalysts and microelectronic device components based on disulfide nanostructures.
E.A.Goodilin. Corresponding Member of the Russian Academy of Sciences, Doctor of Chemical Sciences, Professor, Deputy Dean, Faculty of Materials Science, and Professor, Department of Chemistry, MSU.
Telephone: +7 (495) 939 – 4609, e-mail: goodilin@yandex.ru
Current research interests: composite materials for optical sensors and analytical systems, composites based on noble metal nanoparticles and layered materials; metal-air batteries, perovskite solar cells.
K.A.Solntsev. Full Member of the Russian Academy of Sciences, Doctor of Chemical Sciences, Dean, Faculty of Materials Science, MSU, and Director, Baikov Institute of Metallurgy and Materials Science, Russian Academy of Sciences.
Telephone: +7(495) 237 – 9755, e-mail: solntsev@pran.ru
Current research interests: chemistry and technology of ceramic materials, nanocomposite materials, oxidative design of thin-walled ceramics.

Received 14 November 2017
Translation: A.M.Raevskiy

© 2018 Uspekhi Khimii, Russian Academy of Sciences and Turpion Ltd.

1. Introduction

The synthesis of unique carbon nanostructures, first of all fullerenes,[1] carbon nanotubes (CNT)[2] and graphene[3] in the late 20th and the early 21st century gave an impetus to the design of novel classes of nanocomposites and to the search for similar nanostructures based on noncarbon compounds. Preparation of the latter is an important trend of progress in synthetic inorganic chemistry, crystal chemistry and materials science. Despite great expectations for practical applications of carbon nanostructures and composites based on them,[4,5] it is difficult to believe that they will cover all possible application fields.

Noncarbon tubular nanostructures are of considerable interest from the standpoint of both basic and applied research. They allow one to discover new chemical features of certain elements in the Periodic system and to use them in practically valuable areas, *e.g.*, chemical industry, optics, electronics, analytical chemistry, *etc*. The importance of this research area is, in particular, due to interest in the development of new catalytic processes and in the design of data processing devices, sensors and device components for micro- and nanoelectronics. Successful synthesis of tubular and multilayer onion nanoparticles[6,7] formed by molybdenum and tungsten disulfides became a milestone in the development of inorganic nanostructures. Morphologically, both MoS_2 and WS_2 nanotubes (NT) and onion nanostructures (IF)† resemble multi-walled CNT and fullerenes, respectively; however, they also exhibit specific mechanical, catalytic and electronic properties typical of the layered disulfides only.

There is a large pool of literature concerning basic and applied research on nanocomposites based on CNT and other carbon nanostructures. For instance, methods for functionalization of CNT and the impact of CNT on the properties of nanocomposites have been considered in detail in a number of reviews.[8–16] Among various fields of application of CNT-based composites, mention should be made of power generation and energy storage devices including solar cells and Li-ion batteries, ionistors (supercapacitors), as well as sensors, device components for micro- and nanoelectronics, reinforced polymeric structural materials and biomedical technologies.

Various methods for surface functionalization of tubular and onion MoS_2 and WS_2 nanostructures have been developed and reported since the discovery of these particles in 1992. Some of them were analyzed in reviews[17,18] devoted to progress in studies of closed-cage disulfide nanostructures. Considerable attention was also paid to methods for preparation of single-layer disulfide dispersions and fabrication of nanocomposites and intercalation compounds.[19–25] Unfortunately, no reviews devoted to generalization and systematization of methods for surface modification of disulfide nanotubes and onion nanostructures have been reported to date, and there are only a few publications concerned with the functional properties of nanocomposites based on them.[26] At the same time, it is clear that the development of methods for the synthesis of such systems and studies on their morphology and functional properties extend the basic knowledge in chemistry and physics of nanomaterials, inorganic chemistry, nanochemistry, solid state chemistry and provide the basis for the design of new types of practically valuable devices.

In this review we will briefly outline methods of synthesis, structural features of tubular and onion MoS_2 and WS_2 nanostructures and nanocomposites based on them and formulate the principles that allow one to modify the surface of closed-cage disulfide nanostructures using different molecules, nanoparticles and nanolayers in order to control the functional properties of the systems in hand. Here, we integrate the results obtained during a long-standing collaboration involving students, postgraduate students and researchers working at the Faculty of Materials Science, Lomonosov Moscow State University, and at the leading research group in the field of synthesis and studies on disulfide nanostructures headed by the founder of this research area Prof. R.Tenne (Weizmann Institute of Science, Israel).

2. Structural features of MoS_2 and WS_2 nanotubes and onion nanostructures

Molybdenum disulfide and tungsten disulfide are layered transition-metal dichalcogenides whose structure is composed of 6–7 Å thick X–M–X sandwich layers (M is transition metal; X = S, Se, Te), each atomic layer M and X being hexagonally close-packed. The coordination number (CN) of the transition-metal atoms in these layers equals six and corresponds to two possible types of coordination polyhedra, namely, an octahedron (SnS_2 and PtS_2) and a trigonal prism (MoS_2, WS_2 and NbS_2).[27] The coordination polyhedra of the chalcogen atoms (CN 3) in many layered transition-metal dichalcogenides are highly distorted and nonsymmetric. The layered structure of the dichalcogenide crystals results from superimposition of the sandwich layers over one another. The superimposition motif of the chalcogen atomic layers and the distribution of transition-metal atoms in adjacent layers can vary. These features underlie the variety of polytypes of layered transition-metal dichalcogenides. Indeed, one-, two-, three-, four- and six-layer sequences in packing are possible, and even more exotic long-period structures were reported for certain layered dichalcogenides. The crystal structures of transition-metal dichalcogenides have been considered in more detail in a review.[19]

Three structural types were reported for MoS_2, *viz*., a hexagonal, a rhombohedral and a trigonal one (Fig. 1).[19,28] For all of them, the crystal structures consist of S–Mo–S slabs. Atoms within the slabs are bound by ionic bonds with a large contribution of covalent interactions, while the interaction between neighbouring MoS_2 slabs is weak and corresponds to van der Waals forces. The most stable is the hexagonal polytype where molybdenum atoms are surrounded by sulfur atoms in trigonal prismatic fashion. Each layer consists of shared trigonal prisms $\{MoS_6\}$ with the sulfur atoms from the same sandwich layer located above each other when considering the projection along the *z* axis, while molybdenum atoms are at the centres of prisms. The prisms from adjacent layers are arranged antiparallel to each other and stacked in such a manner that molybdenum atoms from one layer are under sulfur atoms from the other layer (see Fig. 1 *b*). As a result, the

† Noncarbon onion-like nanostructures are also known as 'inorganic fullerenes' (IF). This abbreviation will also be used throughout the text.

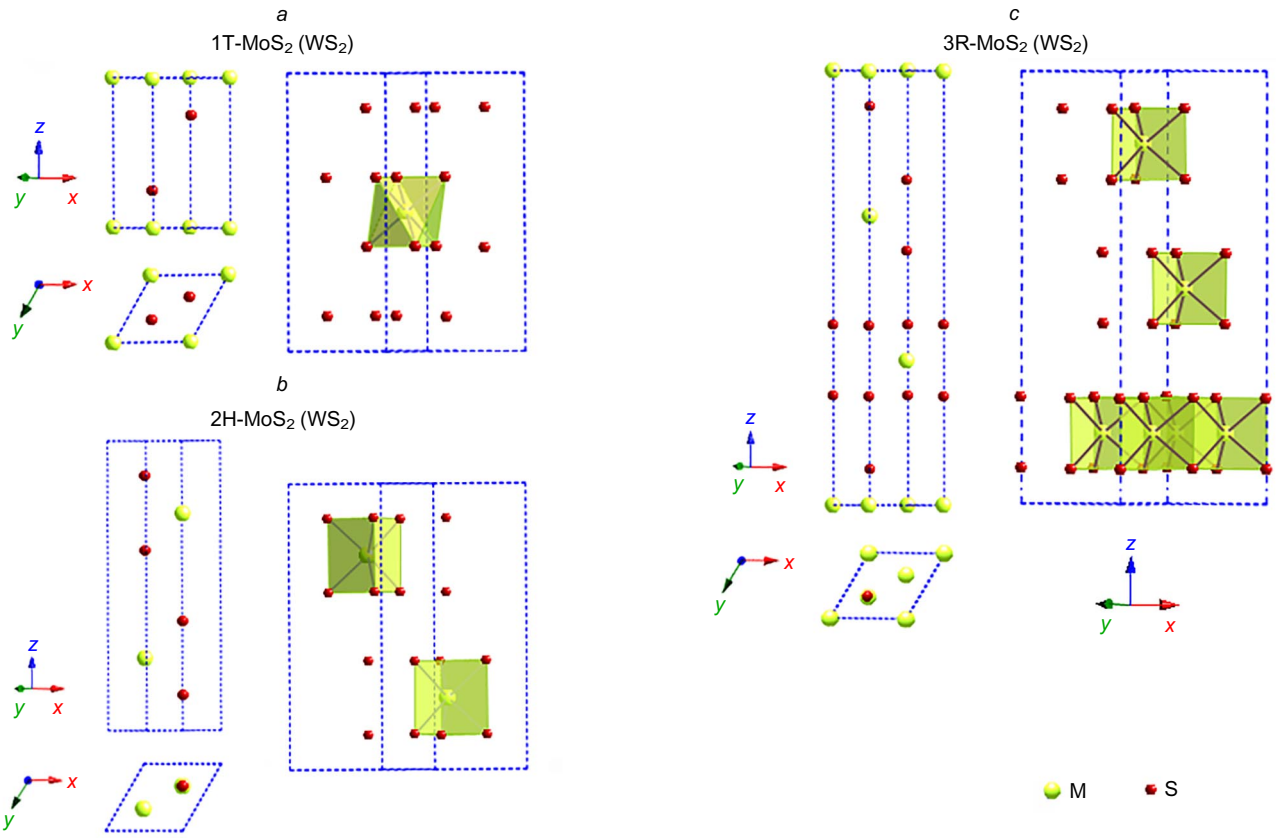


Figure 1. Structural polytypes of molybdenum and tungsten disulfides: 1T (*a*), 2H (*b*) and 3R (*c*). Different unit cell projections (on the left in *a* – *c*) and polyhedral supercells $2a \times 2a$ (on the right in *a* – *c*) are shown.[28]

unit cell of the hexagonal polytype includes two sandwich layers; this polytype is denoted as 2H-MoS_2 (see ‡).

In the rhombohedral polytype of molybdenum disulfide the {MoS_6} trigonal prisms in adjacent layers are arranged parallel to each other; however, only every fourth layer matches the first one (see Fig. 1 *c*). Therefore, the unit cell contains three S – Mo – S layers and the rhombohedral polytype is thus denoted as 3R-MoS_2. Bulk plate-like crystals of 3R-MoS_2 are stable at pressures >4 GPa.[27]

Molybdenum disulfide and tungsten disulfide are isostructural compounds; hexagonal and rhombohedral polymorphs of WS_2 are known. Studies of the alkali metal intercalates A_xMS_2 (A = Li, K; M = Mo, W) made it possible to determine the structures of Li_xMS_2 and K_xMS_2.[29] In these compounds, molybdenum and tungsten atoms are in octahedral environment of sulfur atoms. Hydrolysis and reduction of these intercalates lead to separation into single S – Mo – S layers with trigonal symmetry. Such structures are considered as a particular trigonal polytype with the unit cell containing one sandwich layer (see Fig. 1 *a*); it is denoted as 1T-MoS_2. The formation of metastable multilayer structures 1T-MoS_2 and 1T-WS_2 is governed by the composition of the starting intercalate and by the reducing agents and temperature; however, they undergo an irreversible transformation into the 2H polytype at 95 – 100 °C.[30, 31]

Compounds 2H-MoS_2 and 3R-MoS_2 have nearly equal lattice constants *a* of about 3.16 Å (Table 1); note that $a = b$. The text above and Fig. 1 *a* refer to the ideal structure of the 1T-MoS_2 polytype. Some authors treat the

Table 1. Lattice constants of different MoS_2 and WS_2 polymorphs.[27, 30 – 32]

Compound	*a*/Å	*c*/Å	Space group
1T-MoS_2	3.190	5.945	$P\bar{3}m1$ (see [a])
1T′-MoS_2			
I	5.597	5.994	–
II	6.525	6.14	–
2H-MoS_2	3.160	2×6.147	$P63/mmc$
3R-MoS_2	3.164	3×6.130	$R3m$
2H-WS_2	3.154	2×6.181	$P63/mmc$
3R-WS_2	3.162	3×6.167	$R3m$

Note. Notations are as follows: I stands for the $\sim a_{2H}\sqrt{3} \times a_{2H}\sqrt{3}$ superlattice and II stands for the $\sim 2a_{2H} \times 2a_{2H}$ superlattice.

[a] The lattice constants and the space group of 1T-MoS_2 are given according to Y.Fang, J.Pan, J.He, R.Luo, D.Wang, X.Che, K.Bu, W.Zhao, P.Liu, G.Mu, H.Zhang, T.Lin and F.Huang. *Angew. Chem., Int. Ed.*, **56**, 1 (2017).

‡ Strictly speaking, the notation '2H' refers to the polymorph, while the molybdenum disulfide polytype in question should correctly be referred to as '$2H_c$'. Nevertheless, the two-layer hexagonal polytype of MoS_2 is denoted '2H-MoS_2' for the sake of simplicity.

real structure of trigonal MoS_2 as particular polytype 1T′-MoS_2, where molybdenum atoms are displaced from the centres of the $\{MoS_6\}$ octahedra and form a superlattice. The reported lattice constants of this superlattice vary, namely, $\sim a_{2H}\sqrt{3} \times a_{2H}\sqrt{3}$ (Refs 30, 31) *vs.* $\sim 2a_{2H} \times 2a_{2H}$, where a_{2H} is the lattice constant a of 2H-MoS_2.[32] Correspondingly, the lattice constant a_{1T} equals ~5.6 or ~6.5 Å (see Table 1).

It is a challenge to describe the actual structure of MoS_2 and WS_2, especially, in single-layer dispersions and in layered materials prepared from them, because one deals with nanosized (in some cases, thermodynamically metastable) particles. They can exhibit turbostratic packing of layers and form structures with folded layers. Problems and advances in the synthesis and studies on the structures in question, as well as prospects for application of materials based on them have been thoroughly reviewed.[19]

When studying tubular and onion nanostructures of MoS_2 and WS_2, it is of paramount importance to assign them to a certain polytype of layered transition-metal dichalcogenides. Since each S–M–S layer (M = Mo, W) in the closed-cage structures is bent and shifted relative to the neighbouring layers, the atomic ordering cannot be exactly described using the classical polytypes (1T, 2H and 3R) that assume an ideal translational symmetry. In this connection, the description of tubular and onion nanostructures formed by MoS_2 and WS_2 first of all takes into account the type of the coordination polyhedron of the molybdenum and tungsten atoms (trigonal prism or an octahedron). In the case of trigonal prismatic coordination, the mutual arrangement of the neighbouring layers (parallel or antiparallel) is also analyzed.[33] This approach allows one to describe the alternation defects of the S–M–S layers with trigonal prismatic coordination of metal atoms by combining the 2H and 3R polytypes.

Usually, both types of MoS_2 and WS_2 nanostructures (*i.e.*, NT and IF) are composed of disulfide layers with trigonal prismatic coordination of metal atoms and antiparallel arrangement of slabs. This suggests predominance of the 2H polytype in these nanostructures. At the same time, fragments with parallel arrangement of the S–M–S slabs were identified; they were assigned to the 3R polytype[34,35] which predominates (60%–80%) in IF-WS_2 synthesized by metal organic vapour phase deposition (MOCVD).[34] However, annealing causes the mutual arrangement of slabs to change, so the structure undergoes transformation to the 2H polytype. As noted above, for platelet crystals the 3R polytype is stabilized only at pressures higher than 4 GPa (additionally, it was identified in some natural molybdenite samples[36]). Therefore, the presence of the 3R fragments in the disulfide nanostructures was interpreted as indirect proof of high internal pressures in the tubular and IF nanostructures. A study of rhenium-doped MoS_2 and WS_2 nanotubes revealed the disulfide layers with octahedral coordination of metal atoms, *i.e.*, fragments of the 1T polytype.[37] Similar fragments were also found in the IF structure. It was assumed[38] that the observed 1T layers result from spontaneous transformation 3R → 2H *via* an intermediate 1T phase.

Houben *et al.*[33] reported one of the most thorough studies on the crystal structure of NT-WS_2 and IF-MoS_2. Figure 2 presents the high-resolution transmission electron microscopy (HR TEM) images of NT-WS_2 and the simulated arrangement of tungsten and sulfur atoms in the

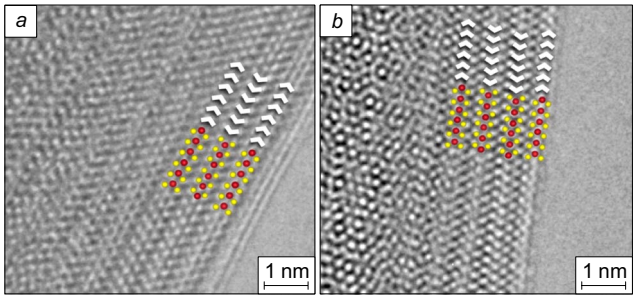


Figure 2. HR TEM images of WS_2 nanotubes.[33] The atomic model overlaid on the images demonstrates the arrangement of tungsten atoms (in red) and sulfur atoms (in yellow) in the 'sandwich' layers: nanotubes with regular antiparallel alignment (conditionally, 2H polytype) (*a*) and two neighbouring S–W–S layers with parallel alignment (conditionally, 3R polytype) (*b*).

observed sandwich layers. The nanotube structure with regular antiparallel alignment of neighbouring layers (see Fig. 2*a*) was attributed to the 2H polytype, whereas neighbouring layers with parallel alignment in NT-WS_2 were treated as a fragment of the 3R polytype (see Fig. 2*b*). An analysis of various HR TEM images showed that the probability to find a parallel alignment of neighbouring layers is nearly 30% irrespective of the particle size and shape (NT or IF) and no regularities in the layer stacking sequence were observed. In this connection, the arrangement of the 3R phase was treated as random and the X-ray diffraction data were analyzed[33] using the Debye equation[39] rather than the classical Rietveld refinement because the former describes diffraction patterns obtained from partially disordered systems as the sum of reflections from a set of aperiodic supercells. The method was used to calculate the theoretical X-ray diffraction patterns of NT-WS_2 and IF-MoS_2 taking into account random distribution of the 2H and 3R polytypes, as well as ordering and bending of the disulfide layers relative to one another. The best agreement between the calculated and experimental X-ray diffraction patterns was obtained using the model which assumed 35% and 40% of randomly distributed 3R phase in NT-WS_2 and IF-MoS_2, respectively.

As in the case of CNT, considerable attention is paid to chirality analysis of NT-MoS_2 and NT-WS_2 and to studies of the impact of chirality on the physicochemical properties of these nanostructures. For instance, nonreciprocal superconductivity in NT-WS_2 was reported for the first time.[40] This nonreciprocity unambiguously shows that superconductivity is related to the chirality of the nanostructure, *viz.*, the forward and backward supercurrents are nonequivalent owing to inversion symmetry breaking.[40] A method for the determination of the chirality of individual multi-walled nanotubes from their electron diffraction patterns and dark-field TEM images was proposed by Margulis *et al.*[41] It was established that some MoS_2 nanotubes prepared by reductive sulfidization of oxide precursors were mono-helical (*i.e.*, all layers had the same chirality). All the mono-helical nanotubes were found to be right-handed and the helicity angles spanned the range from 13 to 29°.

A simulation[33] of the X-ray diffraction patterns of multi-walled NT-WS_2 confirmed correctness of the model which assumes rotation of S–W–S layers by a small angle relative to each other every 6 layers. Based on this, it was

assumed that real NT-WS_2 are composed of blocks of six layers with identical chirality. At the same time, HR TEM studies [42–44] showed that NT-WS_2 with 6 – 8 layers contain single chiral layers sandwiched between same-type (chair or zigzag) blocks of achiral layers.

Bending deformation of disulfide layers in nanotubes and onion nanostructures underlies elastic strain whose compensation requires the appearance of new topological elements or structural defects. As experimental data are accumulated, it becomes increasingly evident that, like carbon nanomaterials, the MoS_2 and WS_2 nanostructures in question should be described using models that take account of lattice defects.[45] Structural defects in MoS_2 and WS_2 nanotubes and onion nanostructures can be classified as follows:

— 0D — vacancies, impurity atoms;

— 1D — dislocations, surface defects (kinks, edges of polygonal onion nanostructures, nanotube steps);

— 2D — stacking defects, grain boundaries; and

— 3D — inner channels in nanotubes and cavities in onion nanostructures.

Lattice defects strongly influence the physical properties and reactivity of nanostructured MoS_2 and WS_2. As shown below, defects play a key role in surface modification of MoS_2 and WS_2 nanotubes and onion nanostructures.

3. Synthesis of MoS_2 and WS_2 nanotubes and onion nanostructures

In 1992, researchers from the group headed by Prof. R. Tenne reported for the first time the formation of WS_2 onion-like nanostructures and multi-walled nanotubes [6] in the course of annealing of tungsten thin films on a quartz substrate in hydrogen sulfide atmosphere at 1000 °C (Fig. 3). More recently, similar molybdenum disulfide nanostructures were prepared by heterogeneous gas-phase sulfidization of the oxide precursor MoO_{3-x} in H_2S atmosphere.[7]

Some pioneering methods for the synthesis of MoS_2 and WS_2 nanostructures were much like those used to obtain high-quality 3D crystals or monolayers of layered transition-metal dichalcogenides. For instance, the first attempts to carry out scalable synthesis of MoS_2 and WS_2 nanotubes involved chemical transport through the gas phase. Metal disulfide powders MS_2 (M = W, Mo) or M and S elements taken in a 1 : 2 ratio, together with transport reagents (usually, bromine or iodine), were placed in the hot zone of an evacuated tube. Then, a single crystal and a small amount of multi-walled micro- and nanotubes of corresponding disulfide grew in the cold zone of the tube within a few days at temperatures 20 – 50 °C lower than that of the hot zone. Optimization of this synthetic approach made it possible to increase the proportion of WS_2 nanotubes compared to particles of other morphology (first of all, plate-like ones), but the duration of the process increased to two weeks and more.[46]

Preparation of MoS_2 nanotubes by template synthesis in pores of anodic aluminium oxide (AAO) was also proposed. Solution deposition of precursor, $(NH_4)_2MoS_4$, into AAO pores was followed by thermal decomposition of the sulfide at 450 °C.[47] The low reaction temperature was chosen because of low thermal stability of AAO; therefore, the resultant nanotubes represented highly defective structures.

The best method for the synthesis of nanostructured MoS_2 and WS_2 involves reductive sulfidization of precursors based on corresponding metal trioxides with specific morphology. For instance, IF structures are prepared using spherical oxide particles, while nanotubes are synthesized from oxide nanorods or nanowhiskers. It should be noted that these methods of synthesis are not related to folding of disulfide layers into closed-cage structures and imply gradual transformations of oxides into disulfides from the surface towards the interior of the precursor particle. The mechanism of formation of IF-MoS_2 and IF-WS_2 is schematically shown in Fig. 4. Its detailed description is available in the literature.[48, 49]

Molybdenum trioxide particles less than 100 nm in size can be prepared *in situ* in a reactor that is used for further sulfidization. To this end, MoO_3 crystals about 5 μm in size are preliminarily evaporated at 700 °C and the obtained oxide vapour reacts first with hydrogen gas (and then with hydrogen sulfide) at a somewhat higher temperature (~820 °C). The volatility of WO_3 is much lower; therefore, the preliminary step during the synthesis of IF-WS_2 is impossible. Tungsten trioxide particles 20 – 200 nm in size that are loaded into a reactor for subsequent sulfidization can be prepared beforehand using various synthetic approaches, *e.g.*, heating of a tungsten filament to 1600 °C in rarefied water vapour atmosphere.

The first stage of sulfidization represents almost instantaneous reductive sulfidization of the MoO_3 surface under the action of $H_2S + H_2$ gas mixture diluted with a carrier gas (usually, nitrogen) at 800 – 950 °C and the formation of an external MoS_2 layer, which precludes sintering of the

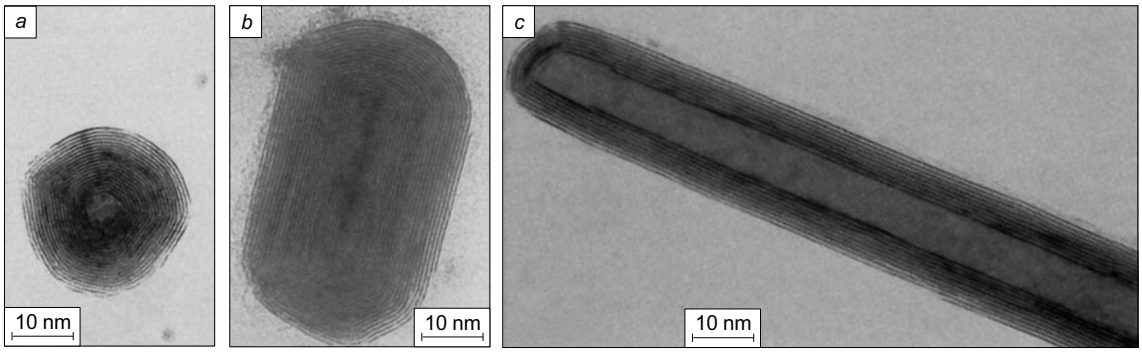


Figure 3. Electron micrographs: WS_2 onion nanostructures (*a*, *b*) and a WS_2 nanotube (*c*).[6]

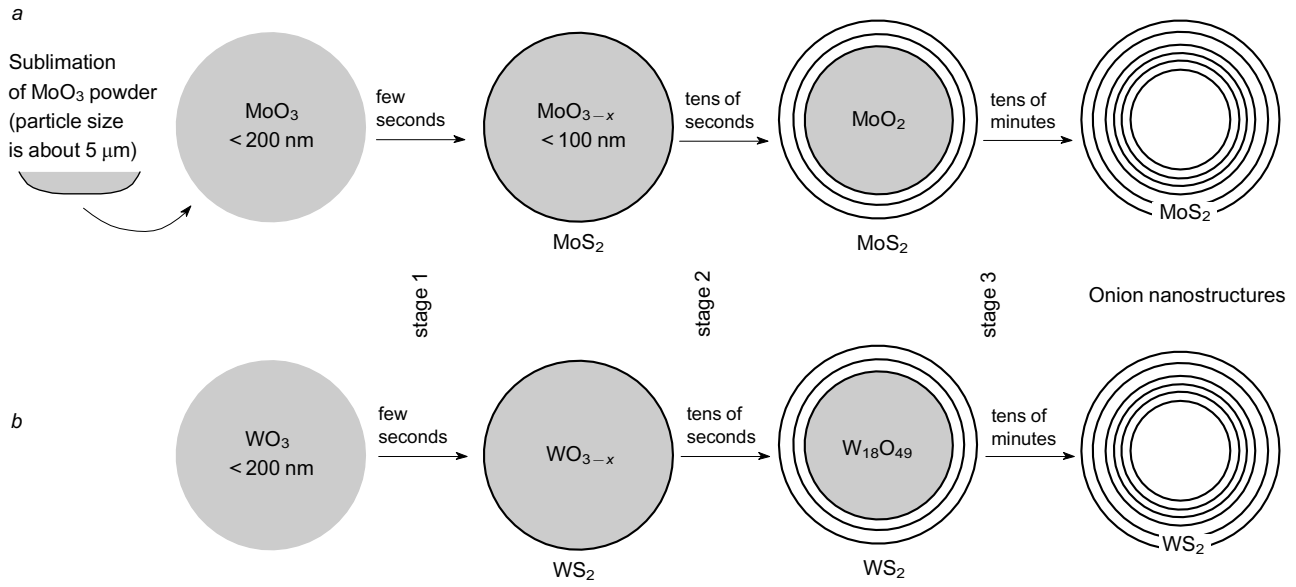


Figure 4. Growth model for IF-MoS_2 (*a*) and IF-WS_2 (*b*) obtained by reductive sulfidization of oxide precursors.[49] The synthesis is carried out in $H_2 + H_2S$ gas mixture diluted with a carrier gas (usually, nitrogen); however, the contributions of hydrogen and hydrogen sulfide to the processes in different stages of the synthesis are different. Namely, the key role is played by the joint action of H_2 and H_2S (stage 1), by the reduction by hydrogen (stage 2) and by sulfidization using hydrogen sulfide (stage 3).

precursor particles. The mechanism of this stage involves successive elimination of three oxygen atoms from the same area of the oxide surface under the action of hydrogen gas. This is followed by relaxation shift of metal atoms in the oxide lattice and formation of chemical bonds between the metal atoms and sulfur atoms from H_2S. At temperatures above 600 °C, this leads to formation of highly ordered monolayers of MoS_2 and WS_2.[50]

The second stage takes a few minutes and involves partial reduction of MO_3 by hydrogen in the interior of the oxide particles. The third stage can take up to a few hours depending on the temperature and particle size of the oxide precursor and represents a diffusion-controlled transformation of the partially reduced oxide core into disulfide mainly under the action of hydrogen sulfide. Sulfidization of the oxide proceeds along a single reaction front which almost steadily moves from the surface inwards. Each next disulfide layer formed plays the role of a template for the formation of the subsequent internal layer (strictly speaking, neighbouring bent MoS_2 or WS_2 layers cannot be crystallographically exactly matched). The densities of the hexavalent molybdenum and tungsten oxides are about 5% lower than those of the corresponding disulfides; *e.g.*, the density of tungsten(VI) oxide is 7.15 g cm^{-3} *vs.* 7.5 g cm^{-3} for tungsten disulfide. Therefore, a complete transformation of oxide into disulfide is accompanied by the appearance of a void at the centre of the particle; this void is clearly seen in the TEM images.

Tungsten oxide whiskers 50 – 300 nm long prepared by heating metallic tungsten filaments in water vapour atmosphere are used as precursor for the synthesis of NT-WS_2.[51 – 53] It should be noted that NT-WS_2 thus synthesized can be significantly different in size from the starting oxide particles because the nanotube growth is influenced by the open-end growth of the starting whiskers, by the reduction of WO_3 and by sulfidization of WO_3 and products of partial reduction of this oxide.

In a highly reductive medium (5% of hydrogen in the gas mixture) the nanotube length is nearly equal to that of the starting WO_3 whiskers. A decrease in the content of hydrogen to 1% provided gradual supply of H_2S is followed by slowing down of the reduction and sulfidization of the oxide. The first disulfide layer covers the entire surface of the whisker except its tips. The formation of the protective disulfide layer on the surface of whiskers is a key step in the synthesis of NT-WS_2. In the absence of this layer the oxide whiskers are reduced to metallic tungsten rods. Since the tips of the whiskers remain uncovered with the disulfide layer, $(WO_3)_n$ and $(WO_{3-x} \cdot H_2O)_n$ clusters with $n \approx 30$ can deposit onto their surface. The role of the source of free tungsten oxide is presumably played by nearly 5-nm oxide nanoparticles representing side products of the reaction between the heated tungsten filament and water vapour that proceeds during the synthesis of the WO_3 whiskers. As these nanoparticles are consumed, the partial pressure of WO_3 in the system decreases, the tips of the whiskers are blocked with the disulfide and the whiskers cease to grow, being 2 – 10 μm long. This parameter is inherited by the newly forming NT-WS_2.

Having tip-growth terminated, diffusion-controlled reduction and sulfidization of the oxide rod in the whiskers become the key processes. Reduction of WO_3 proceeds by the mechanism of crystallographic shift up to the formation of W_3O_8 or $W_{18}O_{49}$. These oxide phases are the most stable ones, their reduction slows down and sulfidization is facilitated, while the outer disulfide layers act as templates for the formation of new inner WS_2 layers.[54, 55] The diameter of the nanotubes matches that of the starting WO_3 whiskers. As in the case of onion nanostructures, the density difference between the oxide and disulfide causes the formation of an inner channel in NT-WS_2. Nanotubes can have either closed or open ends. Formally, the number of S – W – S layers can be varied by varying the duration of synthesis. However, in the case of partial sulfidization the inner

channel of NT-WS_2 will be filled with residues of the oxide phase. This will unavoidably impact the properties of the nanotubes, namely, they will in fact represent a kind of an oxide–sulfide composite material. The size and, indirectly, the number of layers in NT-WS_2 can be varied by changing the diameter of the starting oxide whiskers.

Based on the aforesaid, a method was proposed for the synthesis of mainly open-end NT-WS_2 upto 30 μm long by sulfidization of the $W_{18}O_{49}$ whiskers.[56] Reduction and sulfidization of the $Mo_6S_2I_8$ whiskers afford NT-MoS_2; however, the inner channels in these nanotubes are filled with small amounts of IF-MoS_2.[35]

Industrially scalable synthesis of NT-WS_2 (Refs 57, 58) is also based on the reduction and sulfidization of oxide precursors, namely, nanoparticles of different morphology with the phase composition spanning the range from $WO_{2.83}$ to WO_3. The nanoparticles are loaded into a fluidized bed reactor where they react with the $H_2S + H_2$ gas mixture diluted with a carrier gas (usually, nitrogen). Here, transformations of the oxide to the sulfide are consistent with the mechanism described above; however, it should be augmented with certain preliminary stages corresponding to the growth of oxide nanowhiskers. Unlike the preceding synthetic approach where oxide whiskers grow separately and in advance, here both processes (growth and sulfidization of whiskers) proceed in the same reactor at the same temperature, flow rates and compositions of gas streams.

The mechanism of formation of NT-WS_2 by scalable synthesis in a fluidized bed reactor is schematically shown in Fig. 5 *a*. In stage *I*, the nonvolatile oxide precursor phases $WO_{2.83}-WO_3$ (*1*) are reduced by hydrogen to specific volatile phases WO_x where $2.83 > x > 2.72$ (not precisely defined) (*2*). Initially, particles *2* are close in size to the starting particles *1*; however, they sublime as small molecular clusters owing to the volatile character. Some amount of the sublimed clusters are reduced (stage *II*) to seeds of the nonvolatile phase WO_2 (*3*). Molecular clusters of the nonvolatile WO_2 and volatile WO_x ($2.83 > x > 2.72$) phases are seeds for the growth of $WO_{2.72}$ nanowhiskers (stage *III*). Transformation from the growth to sulfidization of nanowhiskers is a self-controlled process, namely, fast growth of whiskers (within 1–2 min) ceases when the system contains only the reduction-resistant phase $WO_{2.72}$, and then sulfidization under the action of hydrogen sulfide begins. It is assumed that, initially, sulfidization rapidly progresses across the surface of the nanowhiskers from their middle towards the tips (stage *IV*) and then is followed by slow diffusion-controlled motion inwards (stage *V*).

The total synthesis duration is about 6 h and the yield of NT-WS_2 exceeds a value of 95%. The stoichiometric yield of nanotubes is 99% (inner channels of certain nanotubes may be filled with the residual oxide phases). Figures 5 *b* and *c* present an X-ray diffraction pattern and a scanning electron microscopy (SEM) image of NT-WS_2. The size distribution of NT-WS_2 is rather broad, *viz.*, from 5 to 50 μm for the nanotube length and from 20 to 180 nm for the nanotube diameter. Industrial synthesis of IF-MoS_2 and IF-WS_2 is carried out in similar fluidizing bed reactors.[48, 59]

A comparison of the most widely used methods for the synthesis of certain types of nanotubes and onion-like

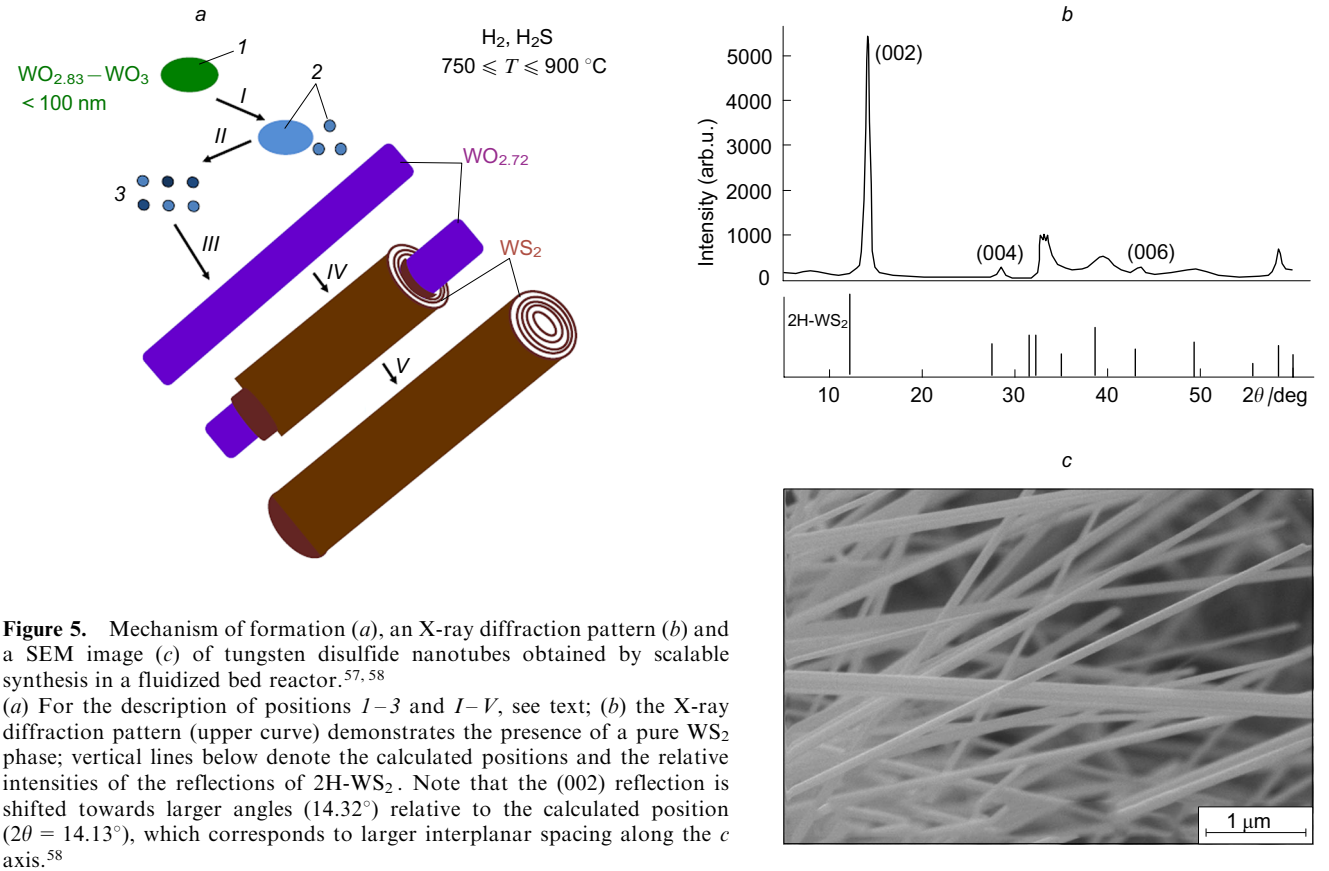


Figure 5. Mechanism of formation (*a*), an X-ray diffraction pattern (*b*) and a SEM image (*c*) of tungsten disulfide nanotubes obtained by scalable synthesis in a fluidized bed reactor.[57, 58]
(*a*) For the description of positions *1*–*3* and *I*–*V*, see text; (*b*) the X-ray diffraction pattern (upper curve) demonstrates the presence of a pure WS_2 phase; vertical lines below denote the calculated positions and the relative intensities of the reflections of 2H-WS_2. Note that the (002) reflection is shifted towards larger angles (14.32°) relative to the calculated position (2θ = 14.13°), which corresponds to larger interplanar spacing along the *c* axis.[58]

structures revealed uniqueness of scalable synthesis by reductive sulfidization of oxide precursors. Seemingly, it is this method that underlies a rapid increase in production and successful commercialization of NT-WS_2 and IF-WS_2. At the same time, CNT and onion nanoparticles, oxide nanotubes and whiskers,[60] NT-BN and other nanostructures are most often synthesized by arc discharge, laser ablation, chemical vapour phase deposition (CVD), solvothermal and template methods, *etc*. (see Table 2). Reductive chalcogenation can be used for the synthesis of small amounts of other chalcogenide nanotubes. For instance, reductive sulfidization of hydroxide precursors was used [18, 61, 62] to prepare nanotubes based on layered misfit compounds, namely, inorganic supramolecular structures with incommensurate structural elements.[63] In some sense the synthesis of BN nanotubes by the substitution reaction [64]

$$B_2O_3 + 3\,C_{NT} + N_2 \longrightarrow 2\,BN_{NT} + 3\,CO$$

is an analogue to the synthesis of dichalcogenide nanostructures from oxide precursors.

However, this reaction is of limited use since one should maintain a high temperature (1260 – 1500 °C) and reaction products include unreacted carbon.[65, 66] Similar processes involving CNT can be used to synthesize carbide tubular nanoparticles (NbC, SiC, TiC); however, all of them proceed in autoclaves at high temperatures [67 – 69] and, usually, the yield of nanotubes is low (Table 2).

There are various less widespread experimental methods for the synthesis of tubular and onion nanostructures of MoS_2 and WS_2. Closed-cage nanostructures can form as side products in the synthesis of bulk and highly disperse molybdenum and tungsten disulfides. A small amount of closed-cage MoS_2 structures with lamellar morphology (intermediate between IF and NT) was found in non-homogeneous MoS_2 [98] synthesized by thermal decomposition of $(NH_4)_2Mo_3S_{13} \cdot x\,H_2O$ at about 400 °C. Imperfect IF-MoS_2 and IF-WS_2 are formed under microwave irradiation of $Mo(CO)_6$ and $W(CO)_6$ vapours in a 1% H_2S + 99% Ar gas mixture at 580 °C. Laboratory-scale amounts of tubular and onion nanostructures of MoS_2 and WS_2 can be obtained by pyrolysis of aerosols, by laser ablation,[99] as well as by MOCVD and CVD at atmospheric pressure.[34] The formation of IF-MoS_2 under electron beam irradiation of molybdenum disulfide crystals [100] and under the action of microsecond electrical pulses from the tip of a scanning tunnelling microscope on amorphous MoS_2 was reported.[101] In the latter case, the cavity of the IF-MoS_2 particles is filled with the starting amorphous disulfide, so core – shell nanostructures are thus formed. Similar onion nanostructures with encapsulated amorphous MoS_2 were obtained by sonoelectrochemical synthesis at room temperature.[102] The process was accompanied by the formation of NT-MoS_2.

No reproducible methods for targeted synthesis of single-walled MoS_2 or WS_2 nanotubes have been reported

Table 2. Main methods for the synthesis of certain types of nanotubes and onion nanostructures.

Materials	Key methods	Ref.
MoS_2 and WS_2 nanotubes and onion nanostructures	Reductive sulfidization of oxide precursors (MoO_3, WO_3, *etc*.); thermal decomposition of $(NH_4)_2MoS_4$ and $(NH_4)_2WS_4$; template methods	18, 70
$MoSe_2$, WSe_2, NbS_2 and $NbSe_2$ nanotubes	Reductive sulfidization and selenization of oxide precursors, decomposition of trichalcogenides, transport chemical reactions	70
CdS, CdSe, CdTe and CuS nanotubes	Template methods, sonochemical synthesis, solvothermal synthesis	70
Nanotubes based on layered misfit compounds	Reductive sulfidization of hydroxide precursors, transport chemical reactions	18, 61, 62
CNT	Arc evaporation, pyrolysis, laser ablation of graphite, CVD, template methods, solvothermal synthesis	70 – 72
BN and BCN nanotubes	Arc evaporation, laser ablation, CVD	64 – 66, 70, 73
GaN, Si_3N_4, Cd_3P_2 and Zn_3P_2 nanotubes	Template methods, MOCVD	70
NbC, WC, SiC and TiC nanotubes	Autoclave substitution reactions using CNT, autoclave decomposition of carbonyls	70
NT-SiO_2	Template methods, pyrolysis of silanes, sol – gel synthesis	70, 74
TiO_2 nanotubes and ordered TiO_2 nanotube arrays	Template methods, solvothermal synthesis, anodic oxidation of titanium, atomic layer deposition	70, 75 – 78
NT-VO_x	Template methods, solvothermal synthesis	70, 78 – 81
Al_2O_3, ZnO, MnO_2, ZrO_2, SnO_2, MoO_3, *etc*. nanotubes	Template methods, solvothermal synthesis, CVD, atomic layer deposition, oxidation of metallic nanowires, anodic oxidation of metals (*e.g*., Al and Zr)	70, 73, 78, 82 – 91
(Hydro)silicate nanotubes	Solvothermal synthesis	92 – 96
Metallic nanotubes (metal — Au, Ag, Cu, Pd, Pt, Ni, Co, Fe, *etc*.)	Template methods	70
Carbon nano-onions	Arc discharge, pyrolysis, pyrochemical reactions	97

so far. Single-to-triple-walled NT-WS_2 3 – 7 nm in diameter and 20 – 100 nm long were obtained by plasma ablation of multi-walled NT-WS_2.[103] Problems related to exact control of the number and moreover the chirality of the layers in the multi-walled WS_2 nanotubes as well as to the synthesis of samples with a narrow size distribution of the tubular and onion structures are still to be solved. Promising methods for the synthesis of monodisperse inorganic nanotubes include template syntheses on monodisperse CNT and in cylindrical surfactant, polymer and biopolymer micelles.[104]

4. Principles and methods for modification of tubular and onion nanostructures of molybdenum and tungsten disulfides

Modification of tubular and onion nanostructures of MoS_2 and WS_2 is a promising trend of research, which facilitates the progress in synthetic methods of solid state chemistry and nanochemistry and in the design of novel nanomaterials. In the last-mentioned case, of particular importance is the surface modification of nanostructures, which plays a dual role. First, chemical or structural modification of the surface is used for targeted design of the interface between the nanomaterial and the matrix in order to realize chemical or morphological control of mechanical joints and adhesion. Such a joint can be of great importance for the design of electrochemically or optically active bulk nanocomposites. Next, chemical modification and decoration of the surface with nanoparticles is an efficient method for engineering of multifunctional nanocomposites (in these systems, the physical properties of all components can vary owing to the proximity effect). Considering surface decoration of tubular and onion nanostructures with nanoparticles, an important role of the nanoparticle/NT(IF)/matrix interface should be emphasized. The interfacial layers formed at the joints between the nanoparticles and the disulfide nanostructures can influence the physical and chemical properties of the nanocomposite.[105] This, in particular, concerns catalytic and exchange processes. Taking account of the aforesaid, nanocomposites based on tubular and onion nanostructures of MoS_2 and WS_2 can be divided into two large classes depending on the role played by these nanostructures:

— composites in which the disulfide nanostructures act as fillers in bulk (*e.g.*, polymeric) matrices; and

— composites in which the disulfide nanostructures are decorated with organic molecules and micro- and nanoparticles of other materials.

Etching the surface of CNT and carbon nanostructures with a mixture of concentrated sulfuric and nitric acids leads to formation of numerous carboxyl, epoxy and other functional groups that can be used for surface modification.[106] Unlike this, no universal methods for functionalization of the surface of NT- and IF-MoS_2 (WS_2) are available. Ideally, the outer surface of nanostructured MoS_2 and WS_2 represents a defect-free layer of hexagonally packed sulfur atoms. This to a great extent governs the chemical properties of the surface and the available strategies of surface modification. The surface of the inner cavity in the disulfide nanotubes has a similar structure.

According to these structural and chemical considerations, methods for modification of tubular and onion nanostructures of MoS_2 and WS_2 are based on the following principles:

— binding of modifiers (molecules or particles) to defects on the disulfide surface (in some cases, one should form nanostructures with high density of surface defects or 'tune' the experimental conditions to improve the reactivity of the available defects);

— the use of linkers anchored to the sulfur surface of the nanostructures and bound to additional functional molecules or nanoparticles;

— maintaining the affinity of sulfur atoms (soft Lewis base) towards soft and (to a lesser extent) borderline Lewis acids including transition-metal cations, metal and metal oxide particles containing transition-metal cation in the surface layer;

— the use of the MoS_2 or WS_2 crystal lattices as templates for growth of other layered materials; and

— filling the inner cavity of disulfide nanotubes with molten modifiers under the action of capillary forces.

Certain methods for modification of nanostructured MoS_2 and WS_2 combine a number of these principles.

4.1. Modification involving surface defects

The first attempts to functionalize the surface of NT- and IF-MoS_2 (WS_2) were aimed at improving their colloidal stability in various solvents and obtaining uniform dispersion in oil and polymeric composites. Pure disulfide nanostructures are highly prone to aggregation. In addition to the expected van der Waals interactions between the disulfide nanoparticles, surface defects and compounds adsorbed from the environment, *e.g.*, water molecules, contribute largely to the mutual adhesion of nanostructures within aggregates.[107]

Long-chain alkylsilane derivatives and n-octadecylphosphonic acid were proposed as modifiers anchored to defects in the surface layer of sulfur atoms. Replacement of the water molecules adsorbed on defects of the disulfide surface by octadecyltrichlorosilane, dodecyltrichlorosilane and hexyltrichlorosilane leads to improvement of the colloidal stability of IF-WS_2 in lubricating oils.[107] Surface modification of NT-WS_2 40 – 50 nm in diameter with n-octadecylphosphonic acid was achieved by sonication in toluene. This led to uniform dispersion of nanotubes in the composite with a polystyrene – poly(methyl methacrylate) copolymer and to a decrease in the number of phase separation domains.[108]

In some cases, the synthesis of polymeric composites with NT- and IF-WS_2 does not require 'masking' of defects in the outer layer of sulfur atoms since it is these defects that are responsible for good adhesion of polymer molecules, *e.g.*, poly(3-hydroxybutyrate), to the nanostructures in hand and for improvement of the mechanical and thermal properties of the composite.[109] Poly(vinylidene fluoride)-*co*-hexafluoropropylene electrospun fibres with embedded NT-WS_2 were reported.[110] Stretching of the material was followed by large shifts of the characteristic vibrational modes in the Raman spectra of NT-WS_2. This confirmed efficient transfer of mechanical load from the polymer to the disulfide filler due to good adhesion of the copolymer to the nanotubes.

Surface defects also play an important role in the modification of disulfide nanostructures with inorganic nanoparticles. For instance, NT-WS_2 was modified with two types of quantum dots, namely, core – shell (CdTe/CdSe) and core – shell – shell (CdSe/CdS/ZnS).[111] At relatively low density of quantum dots, they adsorbed onto

defects on the nanotube surface. At higher density of the chalcogenide quantum dots, they uniformly covered the surface of NT-WS_2. If the fluorescence energy of quantum dots exceeds the bandgap of WS_2, fluorescent resonant (Förster) energy transfer occurs from the quantum dots to the nanotubes in, *e.g.*, the CdSe/CdS/ZnS@NT-WS_2 composites.[111]

4.2. Functionalization using Pearson's concept

There are plenty of methods for modification of nanostructured MoS_2 and WS_2 that are based on Pearson's concept of hard and soft Lewis acids and bases. Soft Lewis bases (platinum, gold, palladium, *etc*. nanoparticles) exhibit the highest affinity to sulfur atoms in the surface layer of disulfide nanostructures. Cations of metals of borderline hardness and nanoparticles bearing such cations are characterized by weaker bonding to the surface of tubular and onion-like nanostructures.[112] Pearson's concept can be clearly illustrated by modification of NT-WS_2 with Pt/Fe_3O_4 Janus nanoparticles.[113] When the nanotubes and Janus nanoparticles are mixed in chloroform, the latter irreversibly bind to the disulfide surface through the platinum domain (Fig. 6 *a*). However, masking of platinum with *O*-[2-(3-mercaptopropionylamino)ethyl]-*O*′-methylpolyethylene glycol (see Fig. 6 *b*) precludes this kind of binding and about 90% of the Janus nanoparticles with the masked platinum domain bind to the surface of NT-WS_2 through the Fe_3O_4 domain (see Fig. 6 *c*). In this case, the Pt/Fe_3O_4 nanoparticles can be reversibly detached from the NT-WS_2 surface on heating the Pt/Fe_3O_4@NT-WS_2 composites in the presence of competing ligands containing catechol groups.

Pearson's concept was also used to prepare nanocomposites containing NT-WS_2 and other transition-metal oxides. For instance, reversible functionalization of disulfide nanotubes with magnetic MnO nanoparticles (Fig. 7) was reported.[114] Mixing dispersions of NT-WS_2 and MnO nanobeads in toluene afforded nanocomposites with the disulfide surface uniformly covered with the oxide particles. However, subsequent heating of the nanocomposites in a solution of dopamine in DMF to 60 °C led to removal of the MnO nanoparticles. The dopamine-treated NT-WS_2 could be used for re-functionalization with the MnO particles. The manganese oxide nanoparticles anchored to the NT-

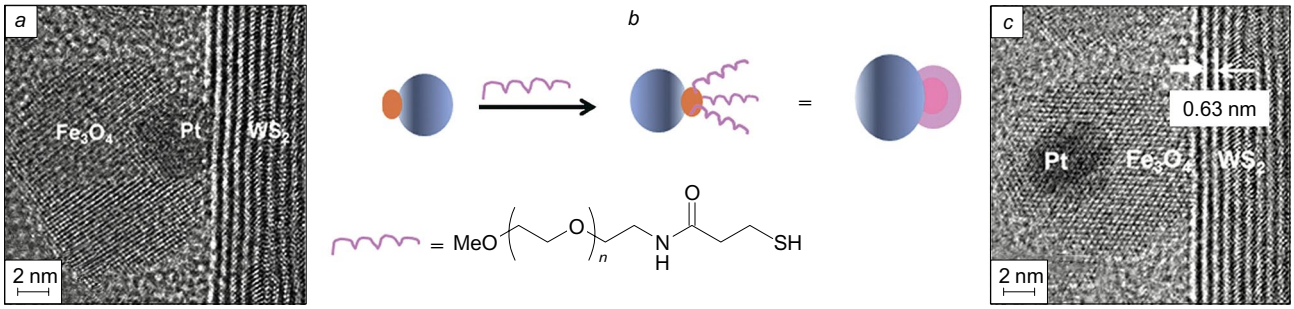


Figure 6. HRTEM images of Pt/Fe_3O_4 Janus nanoparticles bound to the surface of NT-WS_2 (*a*, *c*) and a schematic of masking of the platinum domain in the nanoparticle (*b*).[113]
The platinum domain of the nanoparticle is bound to the surface of NT-WS_2 (*a*); masking of the platinum domain by *O*-[2-(3-mercaptopropionylamino)ethyl]-*O*′-methylpolyethylene glycol (*b*); and the nanoparticle with the masked platinum domain is bound to the surface of NT-WS_2 (*c*).

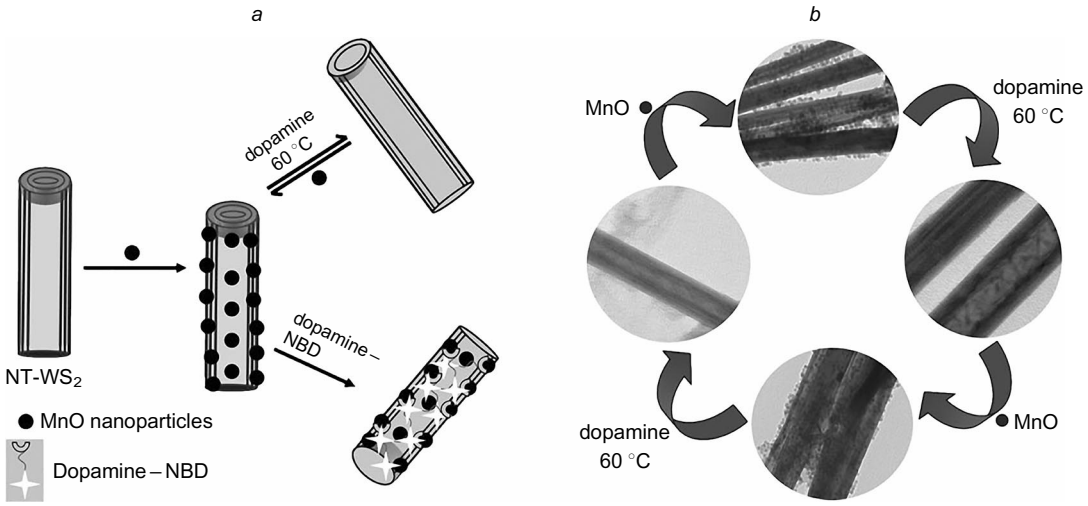


Figure 7. Modification of NT-WS_2 with MnO nanoparticles and NBD fluorescent molecules (*a*) and reversible surface modification of NT-WS_2 with MnO nanoparticles illustrated by TEM images (*b*).[114]

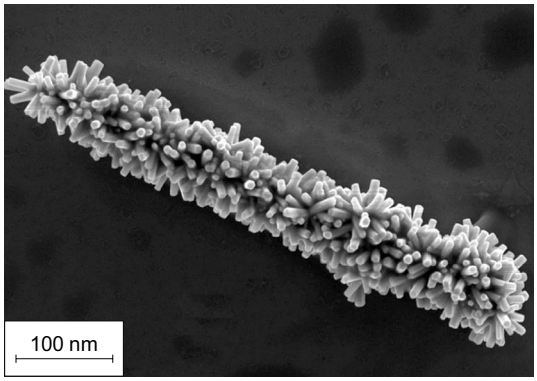


Figure 8. High-resolution SEM image of a brush-like ZnO@NT-WS_2 particle representing NT-WS_2 decorated with ZnO nanorods.[115]

WS_2 surface were used as linkers for further functionalization of the nanocomposite MnO@NT-WS_2 with fluorescent molecules of 7-nitro-4-chlorobenzofurazan (NBD).

Zinc oxide nanoparticles 4 – 5 nm in size were immobilized on the surface of NT-WS_2 and used as seeds to grow an array of ZnO nanorods 100 to 500 nm long and 40 – 50 nm in diameter using the reaction of $Zn(NO_3)_2$ with hexamethylenetetramine.[115] Noteworthy is the unusual brush-like morphology of the ZnO@NT-WS_2 nanocomposites (Fig. 8). These nanocomposites are thought to be promising materials for optoelectronic devices and sensors.

4.3. Pearson's concept for functionalization using linkers

Nanocomposites obtained by combining Pearson's concept and functionalization using linkers were reported by Tahir *et al.*[116 – 118] The linkers were tetradentate nitrilotriacetic ligands attached to the disulfide surface through divalent nickel cations. *In situ* synthesis resulted in a complex where four positions in the octahedral environment of the Ni^{2+} cation were occupied by the nitrilotriacetate ligand while the remaining two positions were occupied by the sulfur atoms from the surface layer of the disulfide nanostructures (Fig. 9). A nitrilotriacetic derivative of fluorescent 7-nitro-4-chlorobenzofurazan was synthesized and used for surface modification of IF-MoS_2.[116] A block copolymer bearing fragments of dopamine and nitrilotriacetic acid molecules (see Fig. 9 *b*) was also synthesized.[116] These fragments provide the possibility to attach the oxide nanoparticles and to anchor to the disulfide surfaces, respectively. This multifunctional polymeric linker was used for immobilization of IF-MoS_2 on the surface of TiO_2 nanorods. In the development of this approach, a multifunctional polymeric ligand with more complicated structure was synthesized.[117] The ligand simultaneously bears fragments of fluorescent 7-nitro-4-chlorobenzofurazan, dopamine and nitrilotriacetate molecules. It was used to prepare fluorescent NT-WS_2 – polymer – TiO_2 (anatase) nanocomposites.

Similar polymeric linkers attached to the disulfide surface through nitrilotriacetic groups and Ni^{2+} cations were used[118] to prepare NT-WS_2/silicatein (protein from marine sponges) conjugates that form stable suspensions in water and organic solvents. The activity of the immobilized silicatein was confirmed by binding silicatein-specific antibodies (PoAb-aSILIC) and by enzymatic hydrolysis of titanium(IV) bis(ammonium lactate) dihydroxide resulting in the formation of a TiO_2 layer.

4.4. Combining Pearson's concept and functionalization of surface defects

Chemisorption of metal and metal oxide nanoparticles onto NT-WS_2 governed by the Pearson's concept can be controlled by the density of defects on the disulfide surface.[45] Experiments with defect-rich NT-WS_2 synthesized by reductive sulfidization of $W_{18}O_{49}$ nanowhiskers showed that functionalization of these nanotubes with metal and metal oxide nanoparticles and with Janus nanoparticles allows one to prepare high-density coatings. The decisive role of the disulfide surface defects was also reported in the studies on functionalization of NT- and IF-WS_2 with pre-synthesized gold nanoparticles (Fig. 10).[45, 119] The formation of chemical bonds between the gold nanoparticles and the surface of the disulfide nanostructures (probably, between the gold atoms and the coordinatively unsaturated sulfur atoms) was pointed out.

Pearson's concept and the reactivity of the surface defects can be used not only for functionalization with pre-synthesized nanoparticles, but also for *in situ* growth

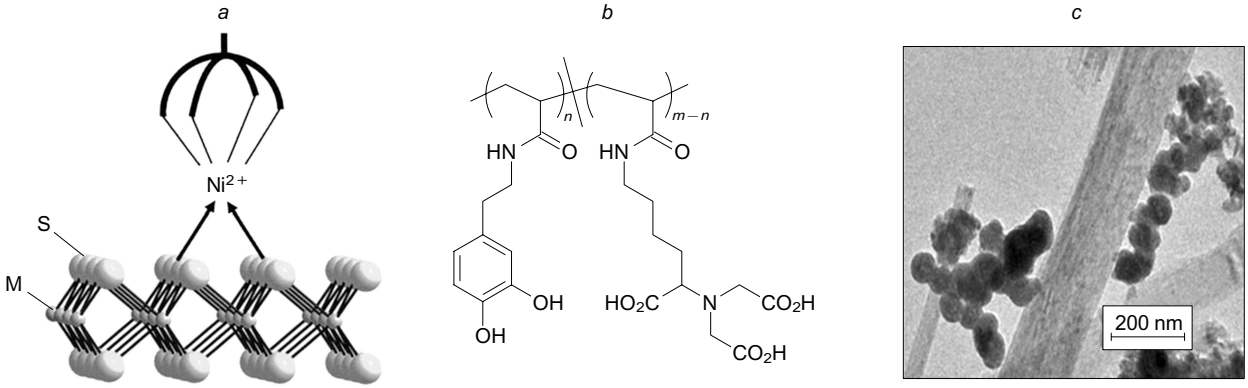


Figure 9. Binding of nitrilotriacetate ligands to the disulfide surface involving Ni^{2+} cation (*a*), the structure of the block copolymer bearing fragments of dopamine and nitrilotriacetic acid molecules (*b*) and a HRTEM image of IF-MoS_2 immobilized on the surface of TiO_2 nanorods using the block copolymer shown in *b* (*c*).[116]

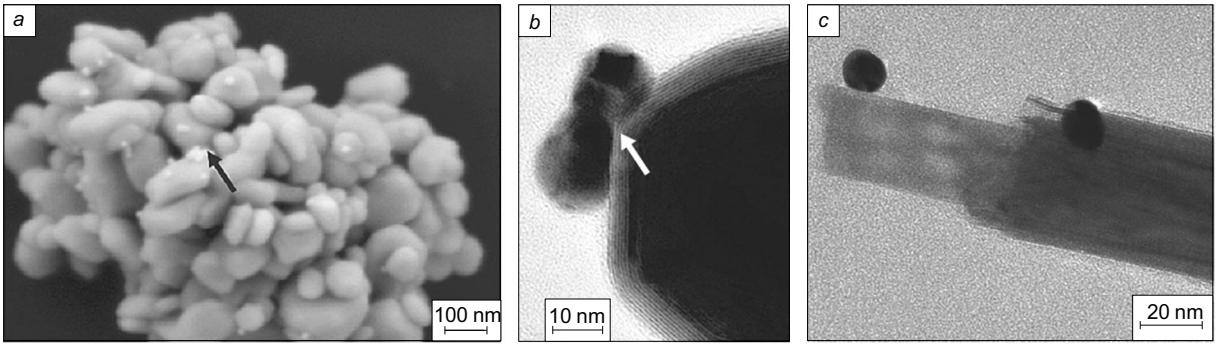


Figure 10. Gold nanoparticles adsorbed on the surface of IF-WS_2: a SEM image (*a*) and a TEM image (*b*) and on the surface of NT-WS_2: a TEM image (*c*).[119] The nanoparticles demonstrate preferred adsorption onto large surface defects of the disulfide nanostructures, namely, IF edges and corners (arrowed) and NT tips.

of nanoparticles on the surface of NT- or IF-MoS_2 and WS_2.

In situ modification of NT-WS_2 with iron oxyhydroxides precipitated from aqueous $FeCl_3$ solution in the presence of NaOH, followed by heating the reaction mixture to 81 °C was reported.[120] The role of defects in the adsorption of $FeOOH/Fe(OH)_3$ onto the nanotube surface was highlighted. It was assumed that step-like defects as well as the nanotube open ends and kinks contain reactive tungsten atoms that can adsorb water and oxygen-containing compounds including highly disperse iron oxyhydroxide particles. Annealing of the $FeOOH/Fe(OH)_3$@NT-WS_2 nanomaterial in inert atmosphere (600 °C, 14 h) resulted in the magnetic composites $FeWO_4$@NT-WS_2.

Reduction of Ni^{2+} cations by citrate anions in the presence of NT-MoS_2 led to *in situ* formation of nanocomposites Ni@NT-MoS_2.[121] More complicated procedures were developed to modify NT-WS_2 with cobalt[122] and nickel.[123] In the former case, the procedure involved a new step, *viz.*, pre-activation of the nanotube surface by treatment with acidified (HCl) aqueous solutions of $SnCl_2$ and then $PdCl_2$.[122] This surface activation technique was reported earlier[124] taking CNT as an example and led to formation of a seed layer of tin and palladium nanoparticles on the CNT surface; the Sn and Pd nanoparticles acted as catalytic sites for subsequent deposition of copper and nickel. It should be noted that reduction of tin and palladium salts probably implies a heterogeneous redox reaction on the surface of the carbon and disulfide nanotubes; however, no detailed studies on the mechanisms of these processes were carried out. Cobalt modification of the activated NT-WS_2 was achieved by inserting the nanotubes into a solution containing $CoCl_2$, $Na_3C_6H_5O_7$, $(CH_3)_2NHBH_3$ and NaH_2PO_2 at pH 9.5 and 70 °C.[122] Modification with nickel was also carried out in a multicomponent system containing $NiSO_4$, $Na_3C_6H_5O_7$, NaH_2PO_2, NH_4Cl and $Pb(NO_3)_2$ at pH 9 and 35 °C.[123]

Detailed studies on the growth of nanoparticles on the surface of disulfide nanostructures were carried out taking *in situ* modification of NT-WS_2 and IF-MoS_2 with gold nanoparticles as an example.[125, 126] It was shown that direct interaction of the disulfides with aqueous $HAuCl_4$ solutions without additional reducing agents causes heterogeneous seeding and growth of gold nanoparticles on the surface of NT-WS_2 and IF-MoS_2 (Fig. 11). The nanoparticle size was

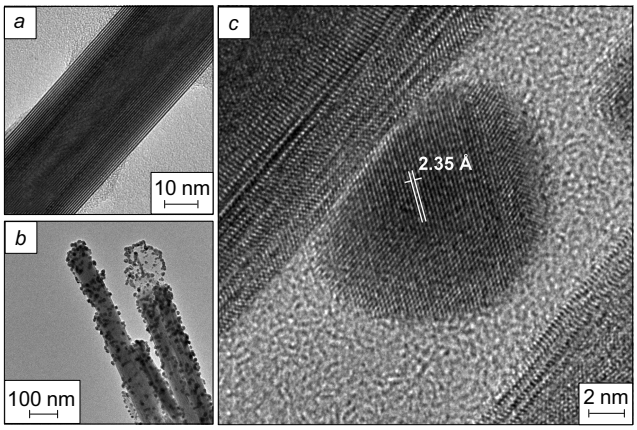


Figure 11. TEM images of pristine NT-WS_2 (*a*) and NT-WS_2 decorated with gold nanoparticles (*b*) and a HRTEM image of the Au/WS_2 interface (*c*).[125]
The distance between the (111) planes of metallic Au is shown.

controllably varied in the range from 5 to 30 nm by varying the concentration of $HAuCl_4$ in the reaction mixture.

It was established that gold nanoparticles are formed near surface defects in the tubular and onion nanostructures (Fig. 12). At room temperature, only the largest defects including nanotube tips and kinks at the 'nano-onion' edges are reactive. At the same time, numerous smaller defects,

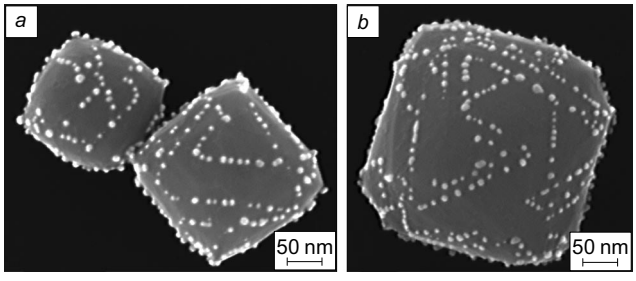


Figure 12. SEM images demonstrating the characteristic arrangement of gold nanoparticles along extended defects of IF-MoS_2.[125]

e.g., steps at the surface of the nanotubes were activated only at elevated temperature (100 °C).

Based on the results of chemical analysis of the reaction mixtures and on the results of microscopy, phase and elemental analyses of reaction products, a mechanism of a heterogeneous reaction of NT-WS_2 and IF-MoS_2 with $HAuCl_4$ was proposed.[125] It involves reduction of $[AuCl_4]^-$ anions and oxidation of MoS_2 and WS_2 to oxides and hydroxides of hexavalent molybdenum and tungsten. It was assumed that reduction of the Au^{3+} ions sorbed from solution can occur at any surface site of the disulfide nanostructure by spontaneous electron transfer from MoS_2 or WS_2 and that the oxidation half-reaction occurs at the nearest defects of the tubular and onion nanostructures where the molybdenum (tungsten) atoms are not terminated with the layer of sulfur atoms. Electron transport between the sites where the oxidation and reduction half-reactions proceed is possible owing to high electronic conductivity of the disulfide layers S–M–S (M = Mo, W).

Spontaneous electron transfer from the disulfide nanostructures to the dissolved trivalent gold compounds is likely driven by the difference between the Fermi level of molybdenum and tungsten disulfides and the reduction potential of $[AuCl_4]^-$ ($[AuCl_4]^- + 3e \rightleftharpoons Au + 4Cl^-$). According to published data (see, *e.g.*, Refs 127–131), the Fermi levels of MoS_2 and WS_2 are 4.6–4.9 eV lower than the vacuum level. The potential of one-electron reduction half-reaction $[AuCl_4]^-$ is 1.002 eV (Refs 132, 133) relative to the standard hydrogen electrode (SHE) potential that lies 4.43–4.48 eV lower than the vacuum level.[134] Thus, the Fermi levels of molybdenum and tungsten disulfides are nearly 0.8 eV higher than the potential of the reduction half-reaction of $[AuCl_4]^-$. As a consequence, one deals with the formation of the $[AuCl_4]^-/MoS_2$ and $[AuCl_4]^-/WS_2$ redox pairs and spontaneous electron transfer (Fig. 13) becomes possible.

A similar mechanism was proposed for spontaneous reduction of $[AuCl_4]^-$ anions on the surface of CNT,[135] graphene[136, 137] as well as MoS_2 and WS_2 nanolayers.[138] Room-temperature partial reduction of Pd^{2+} cations to Pd^0 in the presence of single-layer MoS_2 dispersions was observed.[20] This mechanism is likely in the case of other metal ions with high reduction potential. For instance, a Pd@NT-WS_2 composite was prepared by the reaction of

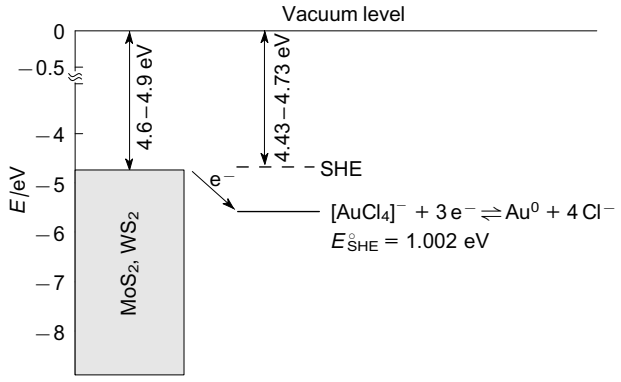


Figure 13. Energy diagram showing the relative positions of the MoS_2 and WS_2 Fermi levels and the standard reduction potential of the $[AuCl_4]^-$ anion.[125]

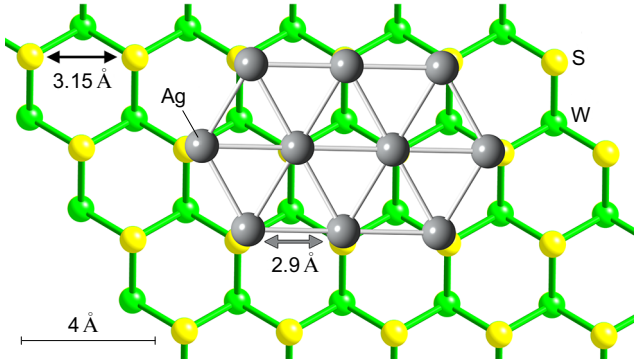


Figure 14. Model for hexagonally packed silver layer formed on the surface of 2H-WS_2.[140]

$Pd_2(DBA)_3$ (DBA is dibenzylideneacetone) with a suspension of NT-WS_2 in toluene at 55 °C.[139] Two wet chemistry techniques developed for functionalization of NT-WS_2 with silver nanoparticles are based on the reaction of NT-WS_2 with aqueous solutions of $AgNO_3$ or $[Ag(NH_3)_2]OH$ at 100 °C.[140] It should be noted that the surface of the MoS_2 and WS_2 nanostructures is a good template for the formation of the Au(111) planes as well as Ag(111) and Pd(111) planes in the cubic polytypes of silver and palladium. For instance, the characteristic interatomic distance in the hexagonally ordered outer layer of sulfur atoms in 2H-WS_2 is 3.15 Å. The distance between gold or silver atoms in the hexagonally close-packed layers corresponding to isostructural Au(111) planes, Ag(111) planes in the cubic polytype of silver and the Ag(004) plane of the hexagonal polytype of silver is only 8% shorter, *viz.*, 2.9 Å (Fig. 14). The structure of the Pd(111) planes in the cubic polytype of palladium (interatomic distance is 2.75 Å) resembles the ordering of sulfur atoms in the surface layer of WS_2 to a lesser extent. It was also found that nanocomposites Ag@NT-WS_2 contain silver nanoparticles with a typical cubic structure 3C-Ag and those belonging to the hexagonal polytype 4H-Ag.[140]

4.5. Capillary wetting and template growth

Capillary wetting is an efficient method for modification of tubular nanostructures. It is specific to this type of systems under study, being widely used for the preparation of core–shell nanocomposites based on NT-WS_2. For instance, a tubular nanocomposite PbI_2–WS_2 was reported.[141] The inner cavity of the WS_2 nanotubes was partially or completely filled with PbI_2. In the former case, concentric PbI_2 layers formed, *i.e.* NT-WS_2 played the role of a template for the formation of the inner NT-PbI_2 (Fig. 15). Capillary wetting was used to prepare analogous composites BiI_3–WS_2 (Fig. 16).[142] The common principle used in this case is to keep mixtures of NT-WS_2 and PbI_2 or BiI_3 (with crystalline iodine added) in an evacuated, sealed quartz tube over a period of 14 to 30 days at 500 °C and then to cool the tube to 0 °C. Wetting of the inner walls of NT-WS_2 was achieved by filling the cavity with molten iodides [$T_m(PbI_2)$ = 410 °C, $T_m(BiI_3)$ = 408 °C] under the action of capillary forces. Cooling of the reaction mixtures led to crystallization of the melts. The tentative mechanism

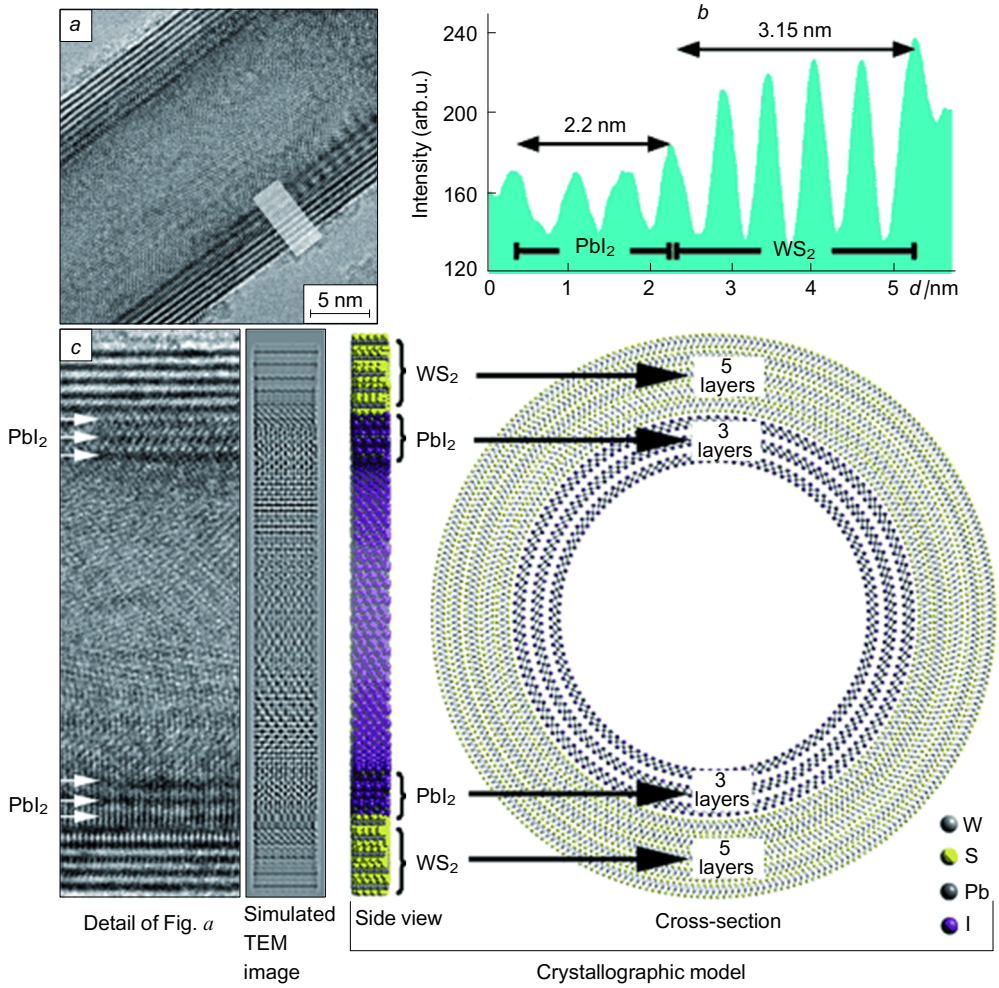


Figure 15. TEM image and a model for the structure of PbI_2-WS_2 nanocomposite prepared by capillary wetting of the inner channel of NT-WS_2 with molten PbI_2.[141]
(*a*) TEM image of tubular composite; white rectangle indicates the region used for calculating the integrated transmitted electron beam intensity profile shown in Fig. *b*.
(*b*) The calculated integrated transmitted electron beam intensity profile used to evaluate the interplanar spacings in the components of the composite.
(*c*) From left to the right shown are a detail from Fig. *a*, a simulated TEM image and a crystallographic model for the PbI_2-WS_2 nanocomposite.

of formation of the PbI_2-WS_2 and BiI_3-WS_2 composites is shown in Fig. 16 *b*.

Also, it was shown that exposure of a mixture of plate-like SbI_3 particles and NT-WS_2 to a focussed electron beam causes the formation of $SbI_3@WS_2@SbI_3$ nanostructures where both the inner and outer surfaces of the disulfide nanotubes are covered with SbI_3.[142] Besides, WS_2 nanotubes were used as templates to grow MoS_2 layers by the gas-phase reaction of $MoCl_5$ with elemental sulfur (800 °C, 6 h), which resulted in the $MoS_2@WS_2$ composite nanotubes.[142]

4.6. Other composites based on tubular and onion nanostructures of MoS_2 and WS_2

In some cases, the method for preparation of a composite based on NT- and IF-MoS_2 does not rigorously obey the principles listed above. For instance, the authors of numerous publications devoted to fabrication of various polymeric materials reinforced with tubular and onion nanostructures of MoS_2 and WS_2 thoroughly discussed the mechanical properties of the composites, whereas specific features of interfaces and interactions between the disulfide nanostructures and polymer matrix were left out of consideration. Examples are provided with reinforcement of poly(methyl methacrylate), polystyrene and isotactic polypropylene with MoS_2 and WS_2 nanotubes.[143,144] Nanocomposites containing NT-WS_2 and biocompatible nylon-11 synthesized from castor oil were reported.[145] Tungsten disulfide nanotubes were used to improve the mechanical properties, chemical and thermal stability of biomaterials based on L-polylactide and hydroxyapatite[146] and poly(propylene fumarate).[147] One can assume that in these cases adhesion of polymers to the unmodified surface of the WS_2 nanotubes is due to the presence of surface defects; however, this still deserves further investigations. Recently, reinforcement of structural materials including cement and

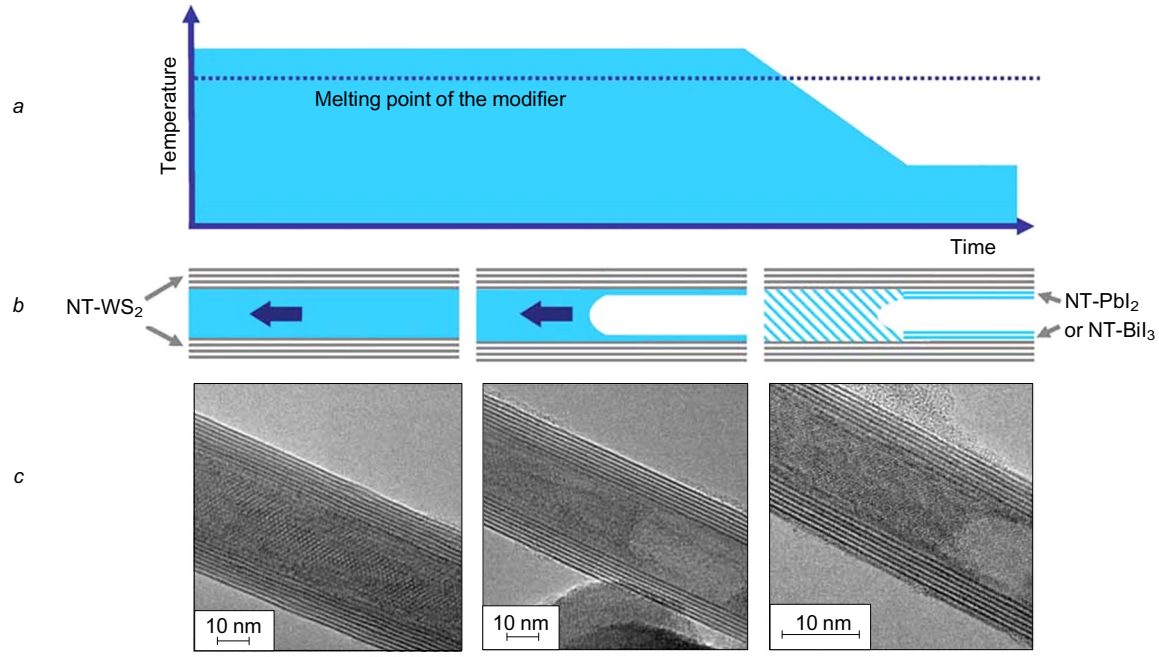


Figure 16. Temperature profile (*a*), a scheme of a tentative mechanism of formation of PbI_2-WS_2 and BiI_3-WS_2 nanocomposites by capillary wetting of the inner channel of NT-WS_2 (*b*) and TEM images of WS_2 nanotubes taken at the corresponding stages of filling with BiI_3 (*c*).[142]
(*b*) Arrows denote the flow direction of the molten iodide along the nanotube channel under the action of capillary forces. Experiments with PbI_2-WS_2 and BiI_3-WS_2 nanocomposites formed by filling the inner channel of NT-WS_2 with molten iodide drops showed that concentric iodide layers do not cover the entire inner channel of NT-WS_2. The remaining volume can be filled with corresponding iodides in the form of nanorods, polycrystalline or amorphized segments (dashed area).

AZ31 magnesium alloy with NT-WS_2 nanotubes was reported.[148, 149]

Uniform dispersion of NT-WS_2 in polymeric nanocomposites is achieved owing to mechanical stiffness of these nanostructures (needle-like morphology is thus retained) and specific dispersion techniques.[57] At the same time, the use of multiply bent § CNT causes entanglement of aggregates and decreases the effective length of the nanotubes.[148]

Recently, studies have begun on the design of composites that simultaneously contain carbon nanomaterials and tungsten (or molybdenum) disulfide nanostructures. For instance, 3D graphene networks containing WS_2 nanotubes incorporated into the interlayer space were synthesized.[150] Coaxial MoS_2 layers coated onto the CNT were used as sacrificial agents for the growth of silver nanoparticles and fabrication of Ag@CNT nanocomposites for antibacterial photocatalysis.[151]

5. Applications of nanocomposites based on tubular and onion nanostructures of molybdenum and tungsten disulfides

Although many studies on the synthesis of nanocomposites based on tubular and onion nanostructures of molybdenum and tungsten disulfides are carried out as part of basic research, a number of materials appeared to be highly efficient in some applications. Information on the actual and potential application fields of these materials is collected in Table 3.

Among them, the most attention is paid to various polymers modified with the MoS_2 and WS_2 nanostructures. Usually, such composites possess improved mechanical and thermal properties [108 – 110, 143, 144, 152] and can be considered as structural materials (including ballistic, stable to local impacts). As mentioned above, NT-WS_2 are used to reinforce other structural materials, in particular, cement [148] and the AZ31 magnesium alloy.[149] Disulfide nanotubes can be used to reinforce polymers that exhibit both structural and functional properties, *e.g.*, nylon-11.[145] In addition to the structural advantages (resistance to liquid hydrocarbon fuels and cryogenic lubricating oils, biocompatibility [159, 160]), nylon-11 exhibits the properties of a piezoelectric.[161, 162]

Multicomponent composites based on L-polylactide and hydroxyapatite reinforced with WS_2 nanotubes appeared to be efficient in bone tissue engineering.[146] Biocompatibility of NT-WS_2 was confirmed in a number of studies.[147, 163, 164] Disulfide nanostructures can also impart specific functional properties to polymeric nanocomposites. For instance, variation of the content of disulfide nanotubes made it possible to improve the mechanical properties of PMMA reinforced with NT-WS_2 (Table 4) and to increase the dielectric constant of the composite.[144] The PMMA/NT-WS_2 nanocomposites thus obtained show the potential for EMI shielding applications.

To date, the best commercialized field of application of tubular and onion nanostructures of MoS_2 and WS_2 has been production of solid lubricants and multicomponent

§ So-called 'spaghetti-like' form.

lubricating mixtures. In this connection, considerable attention is paid to methods for surface modification of disulfide nanostructures aimed at improving their colloidal stability and achieving uniform dispersion in liquid lubricating oils. An example is provided by the improvement of the tribological properties and stability of lubricating mixtures based on IF-WS_2 modified with alkylchlorosilanes.[107] Besides, epoxy resins [153] and polyether ether ketones [154, 155] modified with IF-WS_2 are considered as promising coatings with reduced friction coefficient.

A comparison [153] of the tribological properties of epoxy polymeric composites based on NT-WS_2, IF-WS_2 and platelike particles of 2H-WS_2 deserves attention. An analysis of the results of several tribological tests revealed the worst mechanical properties for the composites with WS_2 platelets. For instance, the coefficient of friction between them and a steel disk exceeded that measured in the tests with the untreated polymer. The lowest value of wear was obtained for the composites containing NT-WS_2, while the lowest coefficient of friction was determined for the composites

Table 3. Application fields of nanocomposites based on MoS_2 and WS_2 nanotubes and onion structures.

Composition	Application field	Ref.
PMMA, polystyrene, isotactic polypropylene, epoxy resins, poly(3-hydroxybutyrate), PVDF – HFP + NT- and IF-MoS_2 and WS_2	Reinforced structural materials, ballistic materials, high-performance adhesives and coatings	108 – 110, 143, 144, 152
Cement composites loaded with NT-WS_2	Reinforced structural materials	148
Magnesium alloy AZ31 + NT-WS_2	Reinforced light metalwork	149
PMMA + NT-WS_2	EMI shielding	144
L-Polylactide + hydroxyapatite + NT-WS_2	Bone tissue engineering	146
Poly(propylene fumarate) + NT-WS_2	The same	147
Nylon-11 + NT-WS_2	Piezoelements, coatings stable to cryogenic oils	145
Epoxy resin + IF-WS_2, poly(ether ether ketone) + IF-WS_2	Polymeric coatings with reduced friction coefficient	153 – 155
Alkyltrichlorosilane@IF-WS_2 (dispersion in lubricating oils)	Multicomponent heterophase lubricating compositions	107
Medical Esracain gel + IF-MoS_2	Antifriction coatings for urological endoscopes	156
Ni@NT-MoS_2	Hydrodesulfurization catalysts	121
Co@NT-WS_2	The same	122
Ni@NT-WS_2	"	123
Co@NT-WS_2	Catalyst with visible-region photocatalytic activity	157
Pd@NT-WS_2	Catalysts of cross-coupling reactions (Heck and Suzuki reactions)	139
Au@NT-WS_2, Au@IF-MoS_2, Ag@NT-WS_2	Optoelectronic devices and sensors	125, 126, 140
ZnO@NT-WS_2	The same	115
$FeWO_4$@NT-WS_2	Filler for magnetic polymers (elastomers)	120
Graphene networks + NT-WS_2	Anode material for Li-ion batteries	150
Rhenium-doped IF-MoS_2	Anode material for Na-ion batteries	158
Tubular composite structures		
$PbI_2 - WS_2$	Nanodetectors of ionizing radiation	141, 142
$BiI_3 - WS_2$	Passive protection against ionizing radiation	141, 142

Note. Notations are as follows: PMMA stands for poly(methyl methacrylate) and PVDF – HFP stands for copolymer poly(vinylidene fluoride) and hexafluoropropylene.

Table 4. Mechanical properties of poly(methyl methacrylate)/NT-WS_2 composites at 26 °C.[144]

Sample	Tensile strength /MPa	Ultimate strain (%)	Young's modulus /MPa	Toughness /MJ m^{-3}
PMMA	1.896	3.29	10.160 ± 0.023	0.0171
PMMA – 1 mass % NT-WS_2	2.56	1.19	102.08 ± 3.60	0.0232
PMMA – 2 mass % NT-WS_2	2.52	0.98	221.47 ± 7.57	0.0123

with IF-WS_2. Improvement of tribological properties was also reported for poly(ether ether ketone) nanocomposites with IF-WS_2.[154, 155] It should be noted that doping with rhenium causes an additional enhancement of the lubricating properties of IF-MoS_2.[165, 166]

Shneider *et al.*[152] studied the peel strength of joints between epoxy resins and the 1100-O aluminium alloy. Experiments with the unmodified epoxy resin gave a peel strength value of 0.0012 kN m^{-1} which more than doubled upon introducing 0.5 mass % IF-WS_2. The dependence of the peel strength on the modifier concentration appeared to be nonmonotonic. At an IF-WS_2 concentration of 0.6 mass %, the peel strength decreased considerably. This suggests the existence of an optimum concentration of disulfide nanostructures at which the adhesive properties of the composites improve significantly.

Preparation of medical lubricating pastes and coatings based on IF-MoS_2 and WS_2 is aimed at reducing the friction of orthodontic wires, endodontic files (drills), urological catheters, stents, *etc.*[156, 167 – 169] This is a relatively new field of application of the systems in question. For instance, lubricants based on medical gels containing rhenium-doped IF-MoS_2 were tested using models for urological endoscopes.[156] The addition of 0.5 mass % – 1 mass % IF-MoS_2 led to reduction of the traction force by more than 50% as the model endoscope passed through the silicone rings simulating human urethra. Surface modification of ureteral stents with a close packed layer of rhenium-doped IF-MoS_2 reduced the traction force between the stent and the surrounding tissues and slowed down encrustation of the surface of the medical device.[169] The biocompatibility of NT- and IF-WS_2 was also studied.[163]

The key application fields of the metal and metal oxide composites with NT- and IF-MoS_2 and WS_2 include catalysis and photocatalysis. Composites containing cobalt and nickel nanoparticles exhibit high activity in hydrodesulfurization of sulfur-containing heterocyclic compounds.[121 – 123] A Co@NT-WS_2 nanocomposite catalyzes hydrodesulfurization of thiophene six times more efficiently than the unmodified composite; however, the catalytic activity of commercially available highly disperse cobalt-doped MoS_2 is four times higher than that of Co@NT-WS_2.[122] The Co@NT-WS_2 composite exhibits high photocatalytic activity upon visible light irradiation.[157] Pd@NT-WS_2 nanocomposites efficiently catalyze cross-coupling reactions (Heck and Suzuki reactions).[139] Besides, nanocomposites Au@NT-WS_2, Au@IF-MoS_2, Ag@NT-WS_2 [125, 126, 140] and ZnO@NT-WS_2 [115] are considered as potential optoelectronic and sensor materials. Since Au and Ag nanoparticles exhibit surface plasmon resonance, composites of disulfide nanostructures with them may appear to be substrates for surface-enhanced Raman scattering (SERS), similarly to already developed SERS-active materials.[170 – 183]

Composites based on tubular and onion nanostructures of molybdenum and tungsten disulfides can be used in the design of novel multicomponent composite materials. For instance, nanocomposites $FeWO_4$@NT-WS_2 are considered as magnetic fillers for magnetic polymers (elastomers).[120] Nanocomposites of NT-WS_2 with heavy-metal iodides, namely, PbI_2-WS_2 and BiI_3-WS_2, are considered as components for materials for the detection of and passive protection against ionizing radiation.[141, 142]

A composite based on 3D stacks of graphene sheets and NT-WS_2 was tested as anode material for Li-ion batteries.[150] The hybrid could maintain an electrochemical capacity of 318.6 mA g^{-1} over 500 cycles at a current density of 1 A g^{-1}. Besides, it was reported that the anode material does not require additional binder and current collector; this will increase the energy density of the cell. Rhenium-doped IF-MoS_2 nanoparticles are considered as promising anode materials for Na-ion batteries with fast charge – discharge.[158] Despite their benefits the MoS_2- and WS_2-based anodes compare poorly with carbon, silicon and metallic (lithium, sodium) anodes in specific electrochemical capacity per unit mass of the electrode. This is due to the high molecular mass of the tungsten and molybdenum disulfides [$M_w(MoS_2) \approx 160$ g mol^{-1}, $M_w(WS_2) \approx 248$ g mol^{-1}] since their intercalation capacity is comparable with that of the carbon nanomaterials. At the same time, taking account of high demand for R&D in electrochemical power industry, these studies preserve their practical usefulness.

6. Conclusion

Since the discovery of tubular and onion nanostructures of molybdenum and tungsten disulfides in 1992,[6] studies on their synthesis, characterization and modification became an independent branch of modern materials science, quite distinct from the research on the corresponding single-layer disulfide materials. Disulfide nanotubes outperform tubular nanosystems formed by other compounds in certain mechanical and electromechanical properties (*e.g.*, Q-factor and torsional frequency), while disulfide onion nanostructures exhibit excellent tribological properties.

Surface modification of the MoS_2 and WS_2 nanostructures as well as their incorporation into various polymeric and inorganic matrices significantly extends the application fields of these disulfide materials. Key features of NT- and IF-MoS_2 and WS_2 that make it possible to prepare nanocomposites based on them include the reactivity of surface defects, the affinity of the sulfur atoms from the outer disulfide layer to soft Lewis acids, and the possibility of epitaxial growth or template synthesis of modifiers on the surface. Also, capillary forces are of great importance for modification of nanotubes because they allow the inner cavity of tubular particles to be filled with molten modifiers. From the standpoint of design of polymeric nanocomposites the advantage of NT-MoS_2 and NT-WS_2 over, *e.g.*, CNT consists in stiffness because this enables more uniform dispersion of the nanotubes in the polymer matrix. For the same reason, NT-WS_2, as constituents of polymeric and cement composites, have a longer effective length compared to the spaghetti-like CNT (provided similar absolute length).

Polymeric nanocomposites based on tubular and, especially, onion nanostructures of MoS_2 and WS_2 offer yet another undoubtful advantage, namely, the antifriction properties. Chemical uniqueness of such nanostructures is manifested in, *e.g.*, their nanocomposites with cobalt and nickel that can catalyze the hydrodesulfurization reactions of heteroaromatic compounds that are unresponsive to other tubular nanocomposite catalysts. Likely, in the nearest future surface modification of NT- and IF-MoS_2 and WS_2 as well as the design of nanocomposites based on them will enable passage from traditional applications of these nanostructures (lubricants, reinforcement of polymers) to innovative ones including fabrication of transistors with

metal-oxide gates, components of optical circuits with nonlinear optical response and nanosensors.

The review has been written with the financial support from the Russian Science Foundation (Project No. 14-13-00871-P); A.Zak expresses her gratitude to the Ministry of Science, Technology & Space, State of Israel (Grant No. 3-11839).

Figure 1 is courtesy of Nature Publishing Group. Figures 2, 5, 8, 10 – 13 are courtesy of American Chemical Society. Figure 3 is courtesy of International Frequency Sensor Association and World Scientific Publishing. Figure 4 is courtesy of Royal Society of Chemistry. Figures 6, 7, 9, 15, 16 are courtesy of John Wiley and Sons. Figure 14 is courtesy of the Publishing House at the St. Petersburg National Research University of Information Technologies, Mechanics and Optics (ITMO University).

References

1. H.W.Kroto, J.R.Heath, S.C.O'Brien, R.F.Curl, R.E.Smalley. *Nature (London)*, **318**, 162 (1985)
2. S.Iijima. *Nature (London)*, **354**, 56 (1991)
3. A.K.Geim, K.S.Novoselov. *Nat. Mater.*, **6**, 183 (2007)
4. A.V.Penkova, S.F.Acquah, L.B.Piotrovskiy, D.A.Markelov, A.S.Semisalova, H.W.Kroto. *Russ. Chem. Rev.*, **86**, 530 (2017)
5. V.N.Postnov, O.V.Rodinkov, L.N.Moskvin, A.G.Novikov, A.S.Bugaichenko, O.A.Krokhina. *Russ. Chem. Rev.*, **85**, 115 (2016)
6. R.Tenne, L.Margulis, M.Genut, G.Hodes. *Nature (London)*, **360**, 444 (1992)
7. Y.Feldman, E.Wasserman, D.J.Srolovitz, R.Tenne. *Science*, **267**, 222 (1995)
8. N.G.Sahoo, S.Rana, J.W.Cho, L.Li, S.H.Chan. *Prog. Polym. Sci.*, **35**, 837 (2010)
9. P.-C.Ma, N.A.Siddiqui, G.Marom, J.-K.Kim. *Composites, Part A: Appl. Sci. Manuf.*, **41**, 1345 (2010)
10. X.Xie, Y.Mai, X.Zhou. *Mater. Sci. Eng. R*, **49**, 89 (2005)
11. Q.Zhang, J.-Q.Huang, W.-Z.Qian, Y.-Y.Zhang, F.Wei. *Small*, **9**, 1237 (2013)
12. Z.Spitalsky, D.Tasis, K.Papagelis, C.Galiotis. *Prog. Polym. Sci.*, **35**, 357 (2010)
13. C.Li, E.T.Thostenson, T.-W.Chou. *Compos. Sci. Technol.*, **68**, 1227 (2008)
14. G.Modugno, C.Ménard-Moyon, M.Prato, A.Bianco. *Br. J. Pharmacol.*, **172**, 975 (2015)
15. E.G.Rakov. *Russ. Chem. Rev.*, **70**, 827 (2001)
16. A.V.Eletskii. *Phys. Usp.*, **40**, 899 (1997)
17. R.Tenne, M.Redlich. *Chem. Soc. Rev.*, **39**, 1423 (2010)
18. R.Tenne. *Front. Phys.*, **9**, 370 (2014)
19. A.S.Golub, Ya.V.Zubavichus, Yu.L.Slovokhotov, Yu.N.Novikov. *Russ. Chem. Rev.*, **72**, 123 (2003)
20. A.S.Golub, Ya.V.Zubavichus, N.D.Lenenko, Yu.L.Slovokhotov, M.Danot, Yu.N.Novikov. *Russ. Chem. Bull., Int. Ed.*, **50**, 2293 (2001)
21. A.S.Golub', D.P.Rupasov, N.D.Lenenko, Y.N.Novikov. *Russ. J. Inorg. Chem.*, **55**, 1166 (2010)
22. Y.A.Kabachii, A.S.Golub, S.Y.Kochev, N.D.Lenenko, S.S.Abramchuk, M.Y.Antipin, P.M.Valetsky, B.D.Stein, W.E.Mahmoud, A.A.Al-Ghamdi, L.M.Bronstein. *Chem. Mater.*, **25**, 2434 (2013)
23. A.S.Golub, N.D.Lenenko, V.I.Zaikovskii, N.N.Efimov, Z.V.Dobrokhotova, A.E.Baranchikov, M.A.Kiskin, I.L.Eremenko. *Mater. Chem. Phys.*, **183**, 457 (2016)
24. I.S.Bushmarinov, A.S.Goloveshkin, N.D.Lenenko, V.I.Zaikovskii, A.A.Korlyukov, A.S.Golub, I.L.Eremenko. *J. Phys. Chem. Lett.*, **7**, 5162 (2016)
25. A.Zak, Y.Feldman, V.Lyakhovitskaya, G.Leitus, R.Popovitz-Biro, E.Wachtel, H.Cohen, S.Reich, R.Tenne. *J. Am. Chem. Soc.*, **124**, 4747 (2002)
26. M.Naffakh, A.M.Díez-Pascual, C.Marco, G.J.Ellis, M.A.Gømez-Fatou. *Prog. Polym. Sci.*, **38**, 1163 (2013)
27. J.A.Wilson, A.D.Yoffe. *Adv. Phys.*, **18**, 193 (1969)
28. G.Du, Z.Guo, S.Wang, R.Zeng, Z.Chen, H.Liu. *Chem. Commun.*, **46**, 1106 (2010)
29. N.Imanishi, M.Toyoda, Y.Takeda, O.Yamamoto. *Solid State Ionics*, **58**, 333 (1992)
30. F.Wypych, R.Schöllhorn. *J. Chem. Soc., Chem. Commun.*, 1386 (1992)
31. F.Wypych, T.Weber, R.Prins. *Chem. Mater.*, **10**, 723 (1998)
32. K.E.Dungey, M.D.Curtis, J.E.Penner-Hahn. *Chem. Mater.*, **10**, 2152 (1998)
33. L.Houben, A.N.Enyashin, Y.Feldman, R.Rosentsveig, D.G.Stroppa, M.Bar-Sadan. *J. Phys. Chem. C*, **116**, 24350 (2012)
34. N.Zink, J.Pansiot, J.Kieffer, H.A.Therese, M.Panthöfer, F.Rocker, U.Kolb, W.Tremel. *Chem. Mater.*, **19**, 6391 (2007)
35. M.Remškar, A.Mrzel, M.Viršek, A.Jesih. *Adv. Mater.*, **19**, 4276 (2007)
36. J.W.Frondel, F.E.Wickman. *Am. Mineral.*, **55**, 1857 (1970)
37. A.N.Enyashin, L.Yadgarov, L.Houben, I.Popov, M.Weidenbach, R.Tenne, M.Bar-Sadan, G.Seifert. *J. Phys. Chem. C*, **115**, 24586 (2011)
38. A.Albu-Yaron, M.Levy, R.Tenne, R.Popovitz-Biro, M.Weidenbach, M.Bar-Sadan, L.Houben, A.N.Enyashin, G.Seifert, D.Feuermann, E.A.Katz, J.M.Gordon. *Angew. Chem., Int. Ed.*, **50**, 1810 (2011)
39. P.Debye. *Ann. Phys.*, **351**, 809 (1915)
40. F.Qin, W.Shi, T.Ideue, M.Yoshida, A.Zak, R.Tenne, T.Kikitsu, D.Inoue, D.Hashizume, Y.Iwasa. *Nat. Commun.*, **8**, 14465 (2017)
41. L.Margulis, P.Dluzewski, Y.Feldman, R.Tenne. *J. Microsc.*, **181**, 68 (1996)
42. M.B.Sadan, L.Houben, A.N.Enyashin, G.Seifert, R.Tenne. *Proc. Natl. Acad. Sci.*, **105**, 15643 (2008)
43. O.Figovsky, D.Pashin, Z.Khalitov, D.Valeeva. *Chem. Chem., Technol.*, **9**, 19 (2015)
44. Z.Khalitov, A.Khadiev, D.Valeeva, D.Pashin. *Acta Crystallogr. Sect. A*, **72**, 36 (2016)
45. W.Tremel, D.Spetter, F.Hoshyargar, J.Sahoo, M.N.Tahir, R.Branscheid, B.Barton, M.Panthöfer, U.Kolb. *Eur. J. Inorg. Chem.*, 2190 (2017)
46. M.Remükar, Z.Škraba, M.Regula. *Adv. Mater.*, **10**, 246 (1998)
47. C.M.Zelenski, P.K.Dorhout. *J. Am. Chem. Soc.*, **120**, 734 (1998)
48. A.Zak, Y.Feldman, V.Alperovich, R.Rosentsveig, R.Tenne. *J. Am. Chem. Soc.*, **122**, 11108 (2000)
49. Y.Feldman, G.L.Frey, M.Homyonfer, V.Lyakhovitskaya, L.Margulis, H.Cohen, G.Hodes, J.L.Hutchison, R.Tenne. *J. Am. Chem. Soc.*, **118**, 5362 (1996)
50. Y.Feldman, V.Lyakhovitskaya, R.Tenne. *J. Am. Chem. Soc.*, **120**, 4176 (1998)
51. A.Rothschild, G.L.Frey, M.Homyonfer, R.Tenne, M.Rappaport. *Mater. Res. Innov.*, **3**, 145 (1999)
52. A.Rothschild, J.Sloan, R.Tenne. *J. Am. Chem. Soc.*, **122**, 5169 (2000)
53. A.Rothschild, R.Popovitz-Biro, O.Lourie, R.Tenne. *J. Phys. Chem. B*, **104**, 8976 (2000)
54. J.Sloan, J.L.Hutchison, R.Tenne, Y.Feldman, T.Tsirlina, M.Homyonfer. *J. Solid State Chem.*, **144**, 100 (1999)
55. A.Margolin, R.Rosentsveig, A.Albu-Yaron, R.Popovitz-Biro, R.Tenne. *J. Mater. Chem.*, **14**, 617 (2004)
56. Y.Q.Zhu, W.K.Hsu, N.Grobert, B.H.Chang, M.Terrones, H.Terrones, H.W.Kroto, D.R.M.Walton, B.Q.Wei. *Chem. Mater.*, **12**, 1190 (2000)

57. A.Zak, L.Sallacan-Ecker, R.Efrati, L.Drangai, N.Fleischer, R.Tenne. *J. Sens. Transduc.*, **12**, 1 (2011)
58. A.Zak, L.Sallacan-Ecker, A.Margolin, M.Genut, R.Tenne. *Nano*, **4**, 91 (2009)
59. Y.Feldman, A.Zak, R.Popovitz-Biro, R.Tenne. *Solid State Sci.*, **2**, 663 (2000)
60. E.A.Goodilin, E.A.Pomerantseva, V.V.Krivetsky, D.M.Itkis, J.Hester, Y.D.Tretyakov. *J. Mater. Chem.*, **15**, 1614 (2005)
61. G.Radovsky, R.Popovitz-Biro, D.G.Stroppa, L.Houben, R.Tenne. *Acc. Chem. Res.*, **47**, 406 (2014)
62. L.S.Panchakarla, G.Radovsky, L.Houben, R.Popovitz-Biro, R.E.Dunin-Borkowski, R.Tenne. *J. Phys. Chem. Lett.*, **5**, 3724 (2014)
63. V.S.Pervov, E.V.Makhonina. *Russ. Chem. Rev.*, **69**, 481 (2000)
64. D.Golberg, W.Han, Y.Bando, L.Bourgeois, K.Kurashima, T.Sato. *J. Appl. Phys.*, **86**, 2364 (1999)
65. S.Kalay, Z.Yilmaz, O.Sen, M.Emanet, E.Kazanc, M.Çulha. *Beilstein J. Nanotechnol.*, **6**, 84 (2015)
66. D.Golberg, Y.Bando, Y.Huang, T.Terao, M.Mitome, C.Tang, C.Zhi. *ACS Nano*, **4**, 2979 (2010)
67. L.Shi, Y.Gu, L.Chen, Z.Yang, J.Ma, Y.Qian. *Carbon*, **43**, 211 (2005)
68. B.Li, R.Wu, Y.Pan, L.Wu, G.Yang, J.Chen, Q.Zhu. *J. Alloys Compd.*, **462**, 446 (2008)
69. T.Taguchi, H.Yamamoto, S.Shamoto. *J. Phys. Chem. C*, **111**, 18888 (2007)
70. *Nanotubes and Nanowires*. (Eds C.N.R.Rao, A.Govindaraj). (Cambridge: Royal Society of Chemistry, 2011)
71. J.Prasek, J.Drbohlavova, J.Chomoucka, J.Hubalek, O.Jasek, V.Adam, R.Kizek. *J. Mater. Chem.*, **21**, 15872 (2011)
72. E.G.Rakov. *Russ. Chem. Rev.*, **69**, 35 (2000)
73. A.L.Ivanovskii. *Russ. Chem. Rev.*, **71**, 175 (2002)
74. B.Polyakov, M.Antsov, S.Vlassov, L.M.Dorogin, M.Vahtrus, R.Zabels, S.Lange, R.Lohmus. *Beilstein J. Nanotechnol.*, **5**, 1808 (2014)
75. D.I.Petukhov, A.A.Eliseev, I.V.Kolesnik, K.S.Napolskii, A.V.Lukashin, A.V.Garshev, Y.D.Tretyakov, D.Chernyshov, W.Bras, S.-F.Chen, C.-P.Liu. *J. Porous Mater.*, **19**, 71 (2012)
76. D.I.Petukhov, A.A.Eliseev, I.V.Kolesnik, K.S.Napolskii, A.V.Lukashin, Y.D.Tretyakov, S.V.Grigoriev, N.A.Grigorieva, H.Eckerlebe. *Microporous Mesoporous Mater.*, **114**, 440 (2008)
77. A.V.Grigorieva, V.V.Yuschenko, I.I.Ivanova, E.A.Goodilin, Y.D.Tretyakov. *J. Nanomater.*, **2012**, Art. ID 920483 (2012)
78. Y.Li, X.-Y.Yang, Y.Feng, Z.-Y.Yuan, B.-L.Su. *Crit. Rev. Solid State Mater. Sci.*, **37**, 1 (2012)
79. S.V.Demishev, A.L.Chernobrovkin, E.A.Goodilin, V.V.Glushkov, A.V.Grigorieva, N.A.Samarin, N.E.Sluchanko, A.V.Semenov, Y.D.Tretyakov. *Phys. Status Solidi — Rapid Res. Lett.*, **2**, 221 (2008)
80. A.V.Grigorieva, E.A.Goodilin, A.V.Anikina, I.V.Kolesnik, Y.D.Tretyakov. *Mendeleev Commun.*, **18**, 71 (2008)
81. A.V.Grigorieva, A.B.Tarasov, E.A.Goodilin, S.M.Badalyan, M.N.Rumyantseva, A.M.Gaskov, A.Birkner, Y.D.Tretyakov. *Mendeleev Commun.*, **18**, 6 (2008)
82. V.V.Pokropivny. *Powder Metall. Met. Ceram.*, **40**, 485 (2001)
83. Y.Tong, Yi.Liu, C.Shao, Y.Liu, C.Xu, J.Zhang, Yu.Lu, D.Shen, X.Fan. *J. Phys. Chem. B*, **110**, 14714 (2006)
84. K.Raidongia, C.N.R.Rao. *J. Phys. Chem. C*, **112**, 13366 (2008)
85. Y.Liu, J.Dong, M.Liu. *Adv. Mater.*, **16**, 353 (2004)
86. N.Du, H.Zhang, B.Chen, X.Ma, D.Yang. *Chem. Commun.*, 3028 (2008)
87. J.Zhao, X.Wang, R.Xu, F.Meng, L.Guo, Y.Li. *Mater. Lett.*, **62**, 4428 (2008)
88. W.Lee, R.Scholz, U.Gösele. *Nano Lett.*, **8**, 2155 (2008)
89. C.-C.Wang, C.-C.Kei, Y.-W.Yu, T.-P.Perng. *Nano Lett.*, **7**, 1566 (2007)
90. J.Luo, H.T.Zhu, H.M.Fan, J.K.Liang, H.L.Shi, G.H.Rao, J.B.Li, Z.M.Du, Z.X.Shen. *J. Phys. Chem. C*, **112**, 12594 (2008)
91. S.Hu, X.Wang. *J. Am. Chem. Soc.*, **130**, 8126 (2008)
92. E.N.Korytkova, L.N.Pivovarova, O.E.Semenova, I.A.Drozdova, V.F.Povinich, V.V.Gusarov. *Russ. J. Inorg. Chem.*, **52**, 338 (2007)
93. E.N.Korytkova, A.V.Maslov, L.N.Pivovarova, Y.V.Polegotchenkova, V.F.Povinich, V.V.Gusarov. *Inorg. Mater.*, **41**, 743 (2005)
94. L.P.Ogorodova, I.A.Kiseleva, E.N.Korytkova, T.P.Maslennikova, V.V.Gusarov. *Russ. J. Phys. Chem. A*, **84**, 44 (2010)
95. A.A.Malkov, E.N.Korytkova, T.P.Maslennikova, A.M.Shtykhova, V.V.Gusarov. *Russ. J. Appl. Chem.*, **82**, 2079 (2009)
96. E.N.Korytkova, L.N.Pivovarova, I.A.Drosdova, V.V.Gusarov. *Russ. J. Gen. Chem.*, **77**, 1669 (2007)
97. J.Bartelmess, S.Giordani. *Beilstein J. Nanotechnol.*, **5**, 1980 (2014)
98. A.Leist, S.Stauf, S.Löken, E.W.Finckh, S.Lödtke, K.K.Unger, W.Assenmacher, W.Mader, W.Tremel. *J. Mater. Chem.*, **8**, 241 (1998)
99. H.Wu, R.Yang, B.Song, Q.Han, J.Li, Y.Zhang, Y.Fang, R.Tenne, C.Wang. *ACS Nano*, **5**, 1276 (2011)
100. M.José-Yacamán, H.López, P.Santiago, D.H.Galván, I.L.Garzón, A.Reyes. *Appl. Phys. Lett.*, **69**, 1065 (1996)
101. M.Homyonfer, Y.Mastai, M.Hershfinkel, V.Volterra, J.L.Hutchison, R.Tenne. *J. Am. Chem. Soc.*, **118**, 7804 (1996)
102. Y.Mastai, M.Homyonfer, A.Gedanken, G.Hodes. *Adv. Mater.*, **11**, 1010 (1999)
103. V.Brüser, R.Popovitz-Biro, A.Albu-Yaron, T.Lorenz, G.Seifert, R.Tenne, A.Zak. *Inorganics*, **2**, 177 (2014)
104. R.Tenne, in *Progress in Inorganic Chemistry*. Vol. 50. (Ed. K.D.Karlin). (New York: Wiley, 2002) p. 269
105. I.S.Flyagina, A.A.Petrov, V.S.Pervov. *Russ. Chem. Rev.*, **85**, 610 (2016)
106. K.Esumi, M.Ishigami, A.Nakajima, K.Sawada, H.Honda. *Carbon*, **34**, 279 (1996)
107. C.Shahar, D.Zbaida, L.Rapoport, H.Cohen, T.Bendikov, J.Tannous, F.Dassenoy, R.Tenne. *Langmuir*, **26**, 4409 (2010)
108. W.Zhang, S.Ge, Y.Wang, M.H.Rafailovich, O.Dhez, D.A.Winesett, H.Ade, K.V.P.M.Shafi, A.Ulman, R.Popovitz-Biro, R.Tenne, J.Sokolov. *Polymer*, **44**, 2109 (2003)
109. M.Naffakh, C.Marco, G.Ellis, S.R.Cohen, A.Laikhtman, L.Rapoport, A.Zak. *Mater. Chem. Phys.*, **147**, 273 (2014)
110. O.Grinberg, S.Deng, E.Zussman, T.Livneh, A.Zak. *Phys. Chem. Chem. Phys.*, **19**, 18443 (2017)
111. R.Kreizman, O.Schwartz, Z.Deutsch, S.Itzhakov, A.Zak, S.R.Cohen, R.Tenne, D.Oron. *Phys. Chem. Chem. Phys.*, **14**, 4271 (2012)
112. M.N.Tahir, A.Yella, J.K.Sahoo, H.Annal-Therese, N.Zink, W.Tremel. *Phys. Status Solidi*, **247**, 2338 (2010)
113. J.K.Sahoo, M.N.Tahir, F.Hoshyargar, B.Nakhjavan, R.Branscheid, U.Kolb, W.Tremel. *Angew. Chem., Int. Ed.*, **50**, 12271 (2011)
114. J.K.Sahoo, M.N.Tahir, A.Yella, T.D.Schladt, E.Mugnaoli, U.Kolb, W.Tremel. *Angew. Chem., Int. Ed.*, **49**, 7578 (2010)
115. M.N.Tahir, A.Yella, H.A.Therese, E.Mugnaioli, M.Panthöfer, H.U.Khan, W.Knoll, U.Kolb, W.Tremel. *Chem. Mater.*, **21**, 5382 (2009)
116. M.N.Tahir, N.Zink, M.Eberhardt, H.A.Therese, U.Kolb, P.Theato, W.Tremel. *Angew. Chem., Int. Ed.*, **45**, 4809 (2006)
117. M.N.Tahir, N.Zink, M.Eberhardt, H.A.Therese, S.Faiss, A.Janshoff, U.Kolb, P.Theato, W.Tremel. *Small*, **3**, 829 (2007)

118. M.N.Tahir, F.Natalio, H.A.Therese, A.Yella, N.Metz, M.R.Shah, E.Mugnaioli, R.Berger, P.Theato, H.-C.Schröder, W.E.G.Müller, W.Tremel. *Adv. Funct. Mater.*, **19**, 285 (2009)
119. C.Shahar, R.Levi, S.R.Cohen, R.Tenne. *J. Phys. Chem. Lett.*, **1**, 540 (2010)
120. A.Sedova, G.Leitus, Y.Feldman, T.Bendikov, R.Popovitz-Biro, S.Khodorov, H.Dodiuk, S.Kenig, R.Tenne. *J. Mater. Sci.*, **52**, 6376 (2017)
121. F.Y.Cheng, J.Chen, X.L.Gou. *Adv. Mater.*, **18**, 2561 (2006)
122. Y.Tsverin, R.Popovitz-Biro, Y.Feldman, R.Tenne, M.R.Komarneni, Z.Yu, A.Chakradhar, A.Sand, U.Burghaus. *Mater. Res. Bull.*, **47**, 1653 (2012)
123. M.R.Komarneni, Z.Yu, U.Burghaus, Y.Tsverin, A.Zak, Y.Feldman, R.Tenne. *Isr. J. Chem.*, **52**, 1053 (2012)
124. L.M.Ang, T.S.A.Hor, G.Q.Xu, C.H.Tung, S.P.Zhao, J.L.S.Wang. *Carbon*, **38**, 363 (2000)
125. A.Y.Polyakov, L.Yadgarov, R.Popovitz-Biro, V.A.Lebedev, I.Pinkas, R.Rosentsveig, Y.Feldman, A.E.Goldt, E.A.Goodilin, R.Tenne. *J. Phys. Chem. C*, **118**, 2161 (2014)
126. A.Y.Polyakov, A.V.Nesterov, A.E.Goldt, V.Zubyuk, T.Dolgova, L.Yadgarov, B.Visic, A.A.Fedyanin, R.Tenne, E.A.Goodilin. *J. Phys., Conf. Ser.*, **643**, 12046 (2015)
127. K.-K.Liu, W.Zhang, Y.-H.Lee, Y.-C.Lin, M.-T.Chang, C.-Y.Su, C.-S.Chang, H.Li, Y.Shi, H.Zhang, C.-S.Lai, L.-J.Li. *Nano Lett.*, **12**, 1538 (2012)
128. J.C.McMenamin, W.E.Spicer. *Phys. Rev. B*, **16**, 5474 (1977)
129. R.Giridharagopal, K.F.Kelly. *ACS Nano*, **2**, 1571 (2008)
130. A.Klein, S.Tiefenbacher, V.Eyert, C.Pettenkofer, W.Jaegermann. *Phys. Rev. B*, **64**, 205416 (2001)
131. W.Jaegermann, F.S.Ohuchi, B.A.Parkinson. *Surf. Sci.*, **201**, 211 (1988)
132. J.J.Lingane. *J. Electroanal. Chem.*, **4**, 332 (1962)
133. M.L.Machesky, W.O.Andrade, A.W.Rose. *Chem. Geol.*, **102**, 53 (1992)
134. H.Reiss, A.Heller. *J. Phys. Chem.*, **89**, 4207 (1985)
135. H.C.Choi, M.Shim, S.Bangsaruntip, H.Dai. *J. Am. Chem. Soc.*, **124**, 9058 (2002)
136. B.-S.Kong, J.Geng, H.-T.Jung. *Chem. Commun.*, 2174 (2009)
137. H.-J.Shin, W.M.Choi, D.Choi, G.H.Han, S.-M.Yoon, H.-K.Park, S.-W.Kim, Y.W.Jin, S.Y.Lee, J.M.Kim, J.-Y.Choi, Y.H.Lee. *J. Am. Chem. Soc.*, **132**, 15603 (2010)
138. J.Kim, S.Byun, A.J.Smith, J.Yu, J.Huang. *J. Phys. Chem. Lett.*, **4**, 1227 (2013)
139. B.Višić, H.Cohen, R.Popovitz-Biro, R.Tenne, V.I.Sokolov, N.V.Abramova, A.G.Buyanovskaya, S.L.Dzvonkovskii, O.L.Lependina. *Chem. – An Asian J.*, **10**, 2234 (2015)
140. A.Y.Polyakov, V.A.Lebedev, L.Yadgarov, E.A.Goodilin. *Nanosyst. Phys., Chem. Math.*, **8**, 628 (2017)
141. R.Kreizman, S.Y.Hong, J.Sloan, R.Popovitz-Biro, A.Albu-Yaron, G.Tobias, B.Ballesteros, B.G.Davis, M.L.H.Green, R.Tenne. *Angew. Chem., Int. Ed.*, **48**, 1230 (2009)
142. R.Kreizman, A.N.Enyashin, F.L.Deepak, A.Albu-Yaron, R.Popovitz-Biro, G.Seifert, R.Tenne. *Adv. Funct. Mater.*, **20**, 2459 (2010)
143. M.Naffakh, M.Remškar, C.Marco, M.A.Gømez-Fatou, I.Jiménez. *J. Mater. Chem.*, **21**, 3574 (2011)
144. C.S.Reddy, A.Zak, E.Zussman. *J. Mater. Chem.*, **21**, 16086 (2011)
145. M.Naffakh, P.S.Shuttleworth, G.Ellis. *RSC Adv.*, **5**, 17879 (2015)
146. M.Naffakh, A.M.Díez-Pascual, B.Zou, J.Chen, Z.Cai, S.Qu, M.Zhu, L.Qian, R.Tenne, D.J.Aframian. *RSC Adv.*, **5**, 65514 (2015)
147. G.Lalwani, A.M.Henslee, B.Farshid, P.Parmar, L.Lin, Y.X.Qin, F.K.Kasper, A.G.Mikos, B.Sitharaman. *Acta Biomater.*, **9**, 8365 (2013)
148. R.Nadiv, M.Shtein, M.Refaeli, A.Peled, O.Regev. *Cem. Concr. Compos.*, **71**, 166 (2016)
149. S.J.Huang, C.H.Ho, Y.Feldman, R.Tenne. *J. Alloys Compd.*, **654**, 15 (2016)
150. R.Chen, T.Zhao, W.Wu, F.Wu, L.Li, J.Qian, R.Xu, H.Wu, H.M.Albishri, A.S.Al-Bogami, D.A.El-Hady, J.Lu, K.Amine. *Nano Lett.*, **14**, 5899 (2014)
151. W.Liu, Y.Feng, H.Tang, H.Yuan, S.He, S.Miao. *Carbon*, **96**, 303 (2016)
152. M.Shneider, H.Dodiuk, S.Kenig, R.Tenne. *J. Adhes. Sci. Technol.*, **24**, 1083 (2010)
153. M.Shneider, L.Rapoport, A.Moshkovich, H.Dodiuk, S.Kenig, R.Tenne, A.Zak. *Phys. Status Solidi*, **210**, 2298 (2013)
154. X.Hou, C.X.Shan, K.-L.Choy. *Surf. Coatings Technol.*, **202**, 2287 (2008)
155. A.M.Díez-Pascual, M.Naffakh, C.Marco, G.Ellis, M.A.Gómez-Fatou. *Prog. Mater. Sci.*, **57**, 1106 (2012)
156. O.Goldbart, A.Sedova, L.Yadgarov, R.Rosentsveig, D.Shumalinsky, L.Lobik, H.D.Wagner, R.Tenne. *Tribol. Lett.*, **55**, 103 (2014)
157. Y.Tsverin, T.Livneh, R.Rosentsveig, A.Zak, I.Pinkas, R.Tenne. *Nanomater. Energy*, **2**, 25 (2013)
158. S.H.Woo, L.Yadgarov, R.Rosentsveig, Y.Park, D.Song, R.Tenne, S.Y.Hong. *Isr. J. Chem.*, **55**, 599 (2015)
159. M.F.Maitz. *Biosurf. Biotribol.*, **1**, 161 (2015)
160. *Polymers: A Property Database, Second Edition*. (Eds B.Ellis, R.Mith). (Boca Raton, FL: CRC Press, 2008)
161. B.A.Newman, P.Chen, K.D.Pae, J.I.Scheinbeim. *J. Appl. Phys.*, **51**, 5161 (1980)
162. A.Datta, Y.S.Choi, E.Chalmers, C.Ou, S.Kar-Narayan. *Adv. Funct. Mater.*, **27**, 1604262 (2017)
163. E.B.Goldman, A.Zak, R.Tenne, E.Kartvelishvily, S.Levin-Zaidman, Y.Neumann, R.Stiubea-Cohen, A.Palmon, A.-H.Hovav, D.J.Aframian. *Tissue Eng., Part A*, **21**, 1013 (2015)
164. M.Pardo, T.Shuster-Meiseles, S.Levin-Zaidman, A.Rudich, Y.Rudich. *Environ. Sci. Technol.*, **48**, 3457 (2014)
165. L.Yadgarov, V.Petrone, R.Rosentsveig, Y.Feldman, R.Tenne, A.Senatore. *Wear*, **297**, 1103 (2013)
166. L.Yadgarov, R.Rosentsveig, G.Leitus, A.Albu-Yaron, A.Moshkovich, V.Perfilyev, R.Vasic, A.I.Frenkel, A.N.Enyashin, G.Seifert, L.Rapoport, R.Tenne. *Angew. Chem., Int. Ed.*, **51**, 1148 (2012)
167. A.R.Adini, M.Redlich, R.Tenne. *J. Mater. Chem.*, **21**, 15121 (2011)
168. O.Goldbart, O.Elianov, D.Shumalinsky, L.Lobik, S.Cytron, R.Rosentsveig, H.D.Wagner, R.Tenne. *Nanoscale*, **5**, 8526 (2013)
169. R.Ron, D.Zbaida, I.Z.Kafka, R.Rosentsveig, I.Leibovitch, R.Tenne. *Nanoscale*, **6**, 5251 (2014)
170. A.S.Sarycheva, V.K.Ivanov, A.E.Baranchikov, S.V.Savilov, A.V.Sidorov, E.A.Goodilin. *RSC Adv.*, **5**, 90335 (2015)
171. A.S.Sarycheva, A.A.Semenova, E.Y.Parshina, N.A.Brazhe, A.Y.Polyakov, A.Y.Kozmenkova, A.V.Grigorieva, G.V.Maksimov, E.A.Goodilin. *Mater. Lett.*, **121**, 66 (2014)
172. A.A.Semenova, N.A.Brazhe, E.Y.Parshina, V.K.Ivanov, G.V.Maksimov, E.A.Goodilin. *Plasmonics*, **9**, 227 (2014)
173. Y.D.Tretyakov, E.A.Goodilin. *Russ. Chem. Rev.*, **78**, 801 (2009)
174. N.A.Brazhe, A.B.Evlyukhin, E.A.Goodilin, A.A.Semenova, S.M.Novikov, S.I.Bozhevolnyi, B.N.Chichkov, A.S.Sarycheva, A.A.Baizhumanov, E.I.Nikelshparg, L.I.Deev, E.G.Maksimov, G.V.Maksimov, O.Sosnovtseva. *Sci. Rep.*, **5**, 13793 (2015)
175. A.Sidorov, O.Vashkinskaya, A.Grigorieva, T.Shekhovtsova, I.Veselova, E.Goodilin. *Chem. Commun.*, **50**, 6468 (2014)
176. A.A.Semenova, N.A.Brazhe, E.Y.Parshina, A.S.Sarycheva, G.V.Maksimov, E.A.Goodilin. *RSC Adv.*, **6**, 85156 (2016)

177. O.E.Eremina, A.V.Sidorov, T.N.Shekhovtsova, E.A.Goodilin, I.A.Veselova. *ACS Appl. Mater. Interfaces*, **9**, 15058 (2017)
178. A.S.Sarycheva, N.A.Brazhe, A.A.Baizhumanov, E.I.Nikelshparg, A.A.Semenova, A.V.Garshev, A.E.Baranchikov, V.K.Ivanov, G.V.Maksimov, O.Sosnovtseva, E.A.Goodilin. *J. Mater. Chem. B*, **4**, 539 (2016)
179. N.V.Suetin, S.A.Evlashin, A.V.Egorov, K.V.Mironovich, S.A.Dagesyan, L.V.Yashina, E.A.Goodilin, V.A.Krivchenko. *Phys. Chem. Chem. Phys.*, **18**, 12344 (2016)
180. A.A.Semenova, E.A.Goodilin, N.A.Brazhe, V.K.Ivanov, A.E.Baranchikov, V.A.Lebedev, A.E.Goldt, O.V.Sosnovtseva, S.V.Savilov, A.V.Egorov, A.R.Brazhe, E.Y.Parshina, O.G.Luneva, G.V.Maksimov, Y.D.Tretyakov. *J. Mater. Chem.*, **22**, 24530 (2012)
181. K.E.Yorov, A.V.Sidorov, A.Y.Polyakov, I.V.Sukhorukova, D.V.Shtansky, W.Grünert, A.V.Grigorieva. *RSC Adv.*, **6**, 39541 (2016)
182. M.O.Volodina, A.Y.Polyakov, A.V.Sidorov, A.V.Grigorieva, E.A.Eremina, S.V.Savilov, E.A.Goodilin. *Mendeleev Commun.*, **26**, 231 (2016)
183. E.Y.Parshina, A.S.Sarycheva, A.I.Yusipovich, N.A.Brazhe, E.A.Goodilin, G.V.Maksimov. *Laser Phys. Lett.*, **10**, 75607 (2013)